CONFIDENTIAL

Copy 256
RM L53J08

NACA RM L53J08

NACA

RESEARCH MEMORANDUM

THE AERODYNAMIC CHARACTERISTICS AT TRANSONIC SPEEDS OF A MODEL WITH A 45° SWEPTBACK WING, INCLUDING THE EFFECT OF LEADING-EDGE SLATS AND A LOW HORIZONTAL TAIL

By Jack F. Runckel and James W. Schmeer

Langley Aeronautical Laboratory
Langley Field, Va.

CLASSIFICATION CHANGED TO UNCLASSIFIED
AUTHORITY: NASA TECHNICAL PUBLICATIONS ANNOUNCEMENTS # 17
EFFECTIVE DATE: MARCH 18, 1960
WHL

CLASSIFIED DOCUMENT

This material contains information affecting the National Defense of the United States within the meaning of the espionage laws, Title 18, U.S.C., Secs. 793 and 794, the transmission or revelation of which in any manner to an unauthorized person is prohibited by law.

NATIONAL ADVISORY COMMITTEE
FOR AERONAUTICS

WASHINGTON
April 5, 1954

CONFIDENTIAL

NATIONAL ADVISORY COMMITTEE FOR AERONAUTICS

RESEARCH MEMORANDUM

THE AERODYNAMIC CHARACTERISTICS AT TRANSONIC SPEEDS OF A MODEL WITH A 45° SWEPTBACK WING, INCLUDING THE EFFECT OF LEADING-EDGE SLATS AND A LOW HORIZONTAL TAIL

By Jack F. Runckel and James W. Schmeer

SUMMARY

An investigation was conducted in the Langley 16-foot transonic tunnel to determine the effects of leading-edge slats on the aerodynamic and longitudinal stability characteristics of a model of a swept-wing fighter-type airplane. The model wing had 45° sweepback of the 0.25-chord line, an aspect ratio of 3.56, a taper ratio of 0.3, and NACA $64_{(06)}A007$ airfoil sections. Two spanwise extents of leading-edge slats were tested, from 35 to 95 percent semispan and from 46 to 95 percent semispan. Both wing-fuselage and complete-model configurations were tested with slats extended and retracted through an angle-of-attack range of 0° to 20° at Mach numbers of 0.60 to 0.97 and from 0° to about 12° at Mach numbers of 1.00 and 1.03.

The use of extended slats at transonic speeds produced increases in lift at high angles of attack, reductions in drag, and increases in lift-drag ratios above moderate lift coefficients when compared to the characteristics for the model with slats retracted. Both slat configurations delayed the onset of instability to higher values of lift coefficient. The addition of the low horizontal tail to the slats-retracted configuration reduced the unstable pitching-moment trends. The 46 to 95 percent-semispan slat configuration with tail was more effective than the slats of longer extent in reducing the pitch-up tendency. Photographs of ink flow in the boundary layer have been used to provide some correlation between the flow changes on the wing and corresponding force and moment changes of the model.

INTRODUCTION

Designers of present-day swept-wing airplanes are generally faced with longitudinal stability and control problems in the transonic-speed range. In addition to the unstable pitching tendencies that occur at these speeds, the margin of thrust available over drag at transonic speeds has generally been small. Increased emphasis, therefore, has been placed on the reduction of drag not only at cruising conditions, but also at higher values of lift occurring during maneuvers.

Leading-edge slats are one of the devices that has been successfully used at low speeds to improve airplane stability and performance at high lift. Tests of swept-wing models with slats at high subsonic speeds have also indicated improvements in lift and drag and longitudinal stability characteristics with slats extended (refs. 1 and 2). The available information on the beneficial effects of leading-edge slats on the aerodynamic characteristics of a 45° sweptback-wing—fuselage combination at transonic speeds has been reported in reference 3. Two spanwise extents of slats were investigated in this reference. The results indicated that gains in lift-drag ratio at high values of lift coefficient were obtained with extended slats. The magnitude of the gain increased with increasing slat span.

The present investigation presents the aerodynamic characteristics at transonic speeds of a 45° sweptback-wing model with tapered leading-edge slats of longer extent than those of reference 3. In addition, the effect on the longitudinal stability of the leading-edge slats in combination with a 45° sweptback horizontal and vertical tail are determined with the horizontal tail located below the wing-chord plane extended. The investigation, which was conducted in the Langley 16-foot transonic tunnel, included tests through an angle-of-attack range from 0° to 20° at Mach numbers of 0.60 to 0.97 and from 0° to about 12° at Mach numbers of 1.00 and 1.03. Slat opening characteristics and loads on the slats obtained during these tests have been presented in reference 4.

SYMBOLS

$b/2$	wing semispan, 2.744 ft
C_D	drag coefficient, D/qS
C_L	lift coefficient, L/qS
$C_{L_{(L/D)max}}$	lift coefficient for maximum lift-drag ratio

C_m	pitching-moment coefficient, $\frac{M_{0.35\bar{c}}}{qS\bar{c}}$
dC_m/dC_L	static-longitudinal-stability parameter
$\bar{c}$	wing mean aerodynamic chord, 1.699 ft
c_s	slat chord (20 percent of local wing chord)
D	drag, lb
L	lift, lb
M	free-stream Mach number
$M_{0.35\bar{c}}$	pitching moment about $0.35\bar{c}$, lb-ft
P_b	base pressure coefficient, $\frac{p_b - p}{q}$
p	free-stream static pressure, lb/sq ft
p_b	static pressure at model base, lb/sq ft
q	free-stream dynamic pressure, lb/sq ft
R	Reynolds number based on $\bar{c}$
S	wing area, 8.46 sq ft
α	angle of attack of fuselage reference line, deg
δ_H	horizontal-tail incidence, deg

Subscripts:

B	basic wing (slats retracted)
S	wing with slats extended
max	maximum

MODEL AND APPARATUS

This investigation was conducted in the Langley 16-foot transonic tunnel which is described in reference 5. The model was attached to the tunnel sting-support system by means of a 6-component internal strain-gage balance. All parts of the model were constructed of aluminum alloy except the canopy, tail fillet, and faired nose section which were made of wood. The wing with slats retracted (basic wing) had 45° sweepback of the 0.25-chord line, taper ratio of 0.3, aspect ratio 3.56, and NACA $64_{(06)}$A007 airfoil sections parallel to the plane of symmetry. The horizontal tail was set at an incidence of -5° for the complete-model tests. For tail-off tests, both the horizontal and vertical tails were removed and a small wooden insert was used to complete the fairing of the canopy to the after end of the fuselage. Photographs of a complete model and a tail-off configuration are shown in figure 1 and a three-view drawing is presented in figure 2. The segmented and tapered slats shown in figure 3 had a chord length of 20 percent of the local wing chord. In a retracted position, the slats were sealed at the trailing edge. In the full-open position the slat segments were extended forward perpendicular to the wing 13-percent-chord line and were deflected 10°. The 35-to-95-percent b/2 slat configuration was formed by extending slat segments 2, 3, 4, and 5; the 46-to-95-percent b/2 slat configuration by extending segments 3,4, and 5. Other model dimensions are listed in table I.

Model base pressures were measured by means of a micromanometer which averaged the pressures from three static-pressure tubes located in the rear duct of the fuselage.

Flow patterns on the upper surface of the wing were obtained by photographing both black nylon tufts cemented on the right wing and ink flow from 8 taps located in the left wing as shown in figure 3. Concurrently with the flow patterns, some shadowgraphs were obtained on the model through the use of a high-intensity mercury-vapor arc as an auxiliary light source. The wings were painted white for flow-visualization runs only. In addition to separate still cameras for ink-flow and tuft pictures, a motion-picture camera was used to photograph the ink flow.

TESTS AND CORRECTIONS TO THE DATA

Six model configurations consisting of the fuselage and basic wing, the fuselage and wing with 35-to-95-percent b/2 slats extended, and the fuselage and wing with 46-to-95-percent b/2 slats extended, each with the tail on and tail off, were tested through an angle-of-attack range

from 0° to 20° at Mach numbers up to and including 0.97 and from 0° to about 12° at Mach numbers of 1.00 and 1.03. Reynolds number, shown in figure 4, varied from 5.2×10^6 to 7.2×10^6 based on the wing mean aerodynamic chord.

Ink-flow and tuft pictures were obtained for the basic wing and the wing with the 35-to-95-percent b/2 slats extended at Mach numbers of 0.60, 0.85, 0.90, 0.95, and 1.00, with the angle of attack varying continuously from 0° to an upper limit imposed by sting-support loads. Still pictures were usually taken at 0.5° increments of sting angle of attack and motion pictures were taken through the entire angle range. Additional pictures were obtained at higher angles of attack by using an auxiliary support system and testing at a fixed sting angle while varying the Mach number.

The angle of attack of the model has been adjusted for sting deflections due to load and therefore the values reported represent the true angles of attack to an estimated ±0.1°. All drag data have been adjusted to a condition of free-stream static pressure at the base of the fuselage. The variation of base pressure coefficient with Mach number at several angles of attack is presented in figure 5 for the fuselage and basic-wing configuration, with and without the tail. Extension of the slats did not affect the base pressures. Other effects of sting interference on the forces and moments were not established for these tests but are known to be small for tail-off configurations (ref. 6). Furthermore, the comparisons of the data for the several complete-model configurations should be valid regardless of the magnitude of the sting tares since the effects in each case would be about the same. Tunnel-wall and blockage effects are also believed to be small and have not been taken into consideration; however, boundary-reflected disturbances may have some effect on the data at supersonic speeds (ref. 7).

The force and moment coefficients obtained with the balance used in this investigation were estimated to be accurate within the following limits:

M	C_L	C_D	C_m
0.60	±0.02	±0.004	±0.004
0.85 to 1.03	±0.01	±0.002	±0.002

RESULTS AND DISCUSSION

The results of the investigation are presented in the following figures:

	Figure
Force and moment characteristics of the complete model	6 to 8
Force and moment characteristics of the wing-fuselage combination	9 to 11
Variation of lift coefficient with Mach number	12
Drag and L/D characteristics	13 to 16
Variation of C_m and dC_m/dC_L with Mach number	17 and 18
Flow-visualization photographs	19 to 28

The comparisons of the presented force and moment data will be confined to complete-model characteristics unless otherwise noted. Data are not presented for a trimmed condition since only one tail incidence was used in the investigation. The flow-visualization photographs were obtained of the model with the tail removed, so the discussion relating flow phenomena to aerodynamic characteristics will refer to the force and moment data of the tail-off configurations.

Lift Characteristics

An inspection of the lift curves of figure 6 reveals that higher values of lift coefficient were obtained for the wing with extended slats at angles of attack above the break in the lift curves for the basic model. This increment in lift at high angles of attack is typical for swept wings with extended slats at both low and high speeds (refs. 1 to 3). The positive lift at zero angle of attack of the tail-off configuration with slats retracted (fig. 9(a)) is due to the effective positive camber of the fuselage (see fig. 2). The variation of lift coefficient with Mach number (fig. 12) is similar for all configurations but shows that the slatted-wing configurations had less lift than the basic wing at low angles of attack due to the downward deflection of the extended leading-edge slats. All configurations have approximately the same lift at $\alpha = 8^\circ$, whereas both slatted wings provide increased lift at higher angles of attack, with the 0.35b/2 to 0.95b/2 slats producing somewhat higher lift increments. Lift-curve slopes ($C_L = 0$ to 0.4) for all configurations were found to be about the same (fig. 6).

Drag Characteristics and Lift-Drag Ratios

The drag polars (fig. 7) show that the reduction in drag at high lift coefficients due to extending the slats persists through the transonic-speed range up to the highest test Mach number. Slats with the longer spanwise extent produced the greater reductions in drag as was found in references 2 and 3. This effect of spanwise extent is further illustrated in figure 13 which indicates that the 35-to-95-percent b/2 slats had lower drag at lift coefficients above 0.6. Below lift coefficients of about 0.4 extending the slats increased the drag. This drag increase would not occur with slats that open and close automatically in this lift range.

The drag increment at zero lift due to the horizontal and vertical tails $\left(\delta_H = -5^\circ\right)$ can be seen in figure 14. It should be noted that this increment will not be the same as for a trimmed condition. The zero-lift drag rise occurs at a Mach number of about 0.93 for all configurations.

Maximum lift-drag ratios presented in figure 15 have not been completely corrected to a support- and interference-free condition but, on a comparative basis, indicate that extending the slats did not cause large reductions in airplane maximum L/D above a Mach number of 0.85. Ratios of L/D attained by the configurations with slats to the L/D for the basic wing configuration are shown in figure 16 and indicate that both slat configurations provide increases in lift-drag ratio above lift coefficients of 0.35 to 0.60 depending on the Mach number and slat configuration. The gains in L/D obtained with slats extended diminished with increases in Mach number. Slats of 35 to 95 percent semispan produced greater increments in L/D than the 0.46b/2 to 0.95b/2 slats at high values of lift coefficient (generally above $C_L = 0.7$ subsonically). The "cross over" lift coefficient $\left((L/D)_S:(L/D)_B = 1.0\right)$ for the 0.35b/2 to 0.95b/2 slat configuration increased progressively from 0.4 at a Mach number of 0.85 to 0.6 at a Mach number of 1.0; the slats with the smaller spanwise extent had a less consistent trend. Obviously, from a performance standpoint the slats should be extended for all values of the ratio $(L/D)_S:(L/D)_B$ greater than 1.0.

Stability Characteristics

The tail-off model with the basic wing exhibited unstable pitching-moment breaks at all Mach numbers (fig. 11(a)). Extension of either the 0.35b/2 to 0.95b/2 or 0.46b/2 to 0.95b/2 slats (figs. 11(b) and (c)) caused more gradual stability changes and extended the abruptly unstable region to higher values of lift coefficient. Delays of the unstable breaks at Mach numbers from 0.85 to 0.97 amounted to 0.1 to 0.2 in lift coefficient. At Mach numbers of 1.00 and 1.03, the lift coefficients

obtained with the slatted wings were not high enough to indicate unstable tendencies.

The addition of the tail to the basic wing-fuselage configuration (figs. 8(a) and 11(a)) reduced the extent of the unstable trends but abrupt instabilities were still present. Extending the 0.35b/2 to 0.95b/2 slats in combination with the low tail resulted in a substantial reduction of pitch-up tendency at a Mach number of 0.60 and an increase of 0.2 to 0.3 in lift coefficient for pitch-up at higher Mach numbers. However, the magnitude of the unstable break was at least as great for the 0.35b/2 to 0.95b/2 slat extended configuration as for the basic model. The 0.46b/2 to 0.95b/2 slat configuration was more effective than the slats of longer extent in reducing the pitch-up tendency at all Mach numbers (fig. 8(b)).

Figure 17 shows that all configurations had essentially the same variation of pitching moment with Mach number. The pitching moments for the model with extended slats were more negative because of the increased loading near the wing tip with slats extended (ref. 3). The variation of static-stability parameter dC_m/dC_L with Mach number (fig. 18) is also similar for all configurations except at a lift coefficient of 0.6 where the basic wing is in the pitch-up region at Mach numbers from 0.85 to 0.95.

Flow-Study Pictures

Ink-flow and tuft pictures are useful aids in determining flow characteristics associated with model force and moment changes. Since no pressure measurements were obtained on the models in this investigation, no complete flow analysis is attempted; however, correlation between the flow phenomena (figs. 19 to 28) and force and moment data will be discussed briefly. In order to aid in understanding how separated flow occurring on various sections of the wing affected longitudinal stability, the pitching-moment axis is drawn on one photograph of each page. In general, the pictures show the regions of separation, indicated by spanwise or rotational flow of the boundary layer and also the position of the shock waves on the wing. The position of the shock waves can be seen not only by the abrupt redirection of the ink flow and tufts but also in some cases, such as at $M = 0.95$, $\alpha = 1.7^\circ$ (fig. 22(a)), by shadowgraph on the surface of the wing and fuselage. Arrows have been added to some of the photographs of figure 22 in order to point out some typical examples of the position of the shocks. Only those shock fronts, which were sufficiently strong at their line of tangency to the rays of the high-intensity mercury-vapor light source, were detected by the shadowgraph method.

Two ink-flow photographs at an angle of attack of 14.4° are included in figure 20(b). The first picture was taken as part of a constant Mach number, continuously varying angle test; the second is the result of a constant angle, varying Mach number test and shows the difference in appearance of the flow pattern due to the latter method of testing. That is, since the flow over the wing was already partially separated at the time of the release of ink, some areas of the wing were not covered. Furthermore, motion pictures showed that, for the slats-retracted configuration, the ink was flowing inboard near the leading edge of the wing at high angles of attack.

In a few cases an abrupt change in stability or lift characteristics can be correlated with a major change in the flow pattern. An example of an abrupt change is noted in the pitching-moment curve for the tail-off, slats-retracted configuration at a Mach number of 0.60 (fig. 11(a)), where an unstable break occurs at $C_L = 0.68$. Figure 19(a) shows that between $C_L = 0.61$ and 0.69 the flow in the boundary layer changed from a generally chordwise direction to a predominantly spanwise direction, indicative of separation over a large area of the wing behind the pitching-moment axis and its associated unstable pitching-moment break. Generally, the changes in the aerodynamic characteristics are more gradual and the flow pictures, too, show gradual changes. For example, the tail-off 35-to-95-percent b/2 slats-extended configuration at a Mach number of 0.60 had gradual changes in both the stability (fig. 11(b)) and the ink-flow pattern (fig. 19(b)). A comparison of these two flow patterns for the slats retracted and extended also shows the effectiveness of the extended slats in delaying separation to a higher angle of attack by as much as 4° or 5°.

The effects of several shock waves on the boundary-layer flow are noted for both wing combinations at Mach numbers of 0.90, 0.95, and 1.00 (figs. 21, 22, and 23). A leading-edge shock at moderate angles of attack and high Mach numbers, for example at angles greater than 5.7° (fig. 23(a)), is indicated by the ink flow bending spanwise near the ink taps. At higher angles of attack the redirection of the flow due to leading-edge shock conforms nearly to a line extending from the juncture of the wing leading edge and the fuselage toward the trailing edge of the wing tip. This leading-edge shock sweeps rearward with increasing angle of attack (ref. 8) and therefore was observed only when the angle of attack was high enough to move the shock behind the ink taps. A second disturbance, termed the trailing-edge shock, swept across the wing from the vicinity of the fuselage-wing trailing-edge juncture. With an increase of Mach number from 0.90 to 1.00, the trailing-edge shock moved toward the trailing edge of the wing as can be seen at an angle of attack of about 5° in figures 21(a), 22(a), and 23(a). A third disturbance, called a decelerating-flow shock (associated with the deceleration of the supersonic flow field about the complete model) occurred very near or coincident with the

trailing-edge shock at a Mach number of 0.90. At a Mach number of 0.95 the decelerating-flow shock moved downstream of the trailing-edge shock and with increasing angle of attack moved off the wing entirely, as evidenced by its shadow across the fuselage (figs. 22(a) and (b)). At a Mach number of 1.00 the decelerating-flow shock was located at the after end of the fuselage and no longer influenced the wing. It is apparent from these flow pictures that the position of shock waves on the wing and fuselage was not greatly affected by extending the slats but the degree of separation associated with the shock fronts appeared to be somewhat reduced. For further description of these disturbances and their effects on the section characteristics of a 45° sweptback wing, see reference 8, and for a study based on pressure distributions, ink-flow pictures, and tuft pictures of the flow over a swept wing with and without leading-edge extensions, see reference 9.

CONCLUSIONS

An investigation of the effect of leading-edge slats of two spanwise extents and of a low horizontal tail on the aerodynamic and longitudinal stability characteristics of a model of a swept-wing fighter-type airplane at transonic speeds has led to the following conclusions:

1. Increases in lift-drag ratio above lift coefficients of 0.35 to 0.6 depending on the Mach number were obtained with both slat configurations when compared to data for the basic model. The gains in lift-drag ratio through the use of slats diminished with increasing Mach number.

2. The addition of the low horizontal tail to the basic wing-fuselage configuration reduced the unstable pitching-moment trends but abrupt instabilities were still present.

3. The combination of the tail with extended 35-to-95-percent-semispan slats generally resulted in an increase of 0.2 to 0.3 in the lift coefficient for pitch-up, but the magnitude of the unstable break was as great as for the basic tail-on model.

4. The 46-to-95-percent-semispan slat configuration with tail was more effective than the slats of longer extent in reducing the pitch-up tendency at all Mach numbers.

Langley Aeronautical Laboratory,
National Advisory Committee for Aeronautics,
Langley Field, Va., September 22, 1953.

REFERENCES

1. Kelly, John A., and Mayter, Nora-Lee F.: Aerodynamic Characteristics of a Leading-Edge Slat on a 35° Swept-Back Wing for Mach Numbers From 0.30 to 0.88. NACA RM A51H23, 1951.

2. Kennedy, J.: Report on Additional Wind Tunnel Tests of a 0.15-Scale Reflection-Plane Model of the North American, Inglewood, F-100A Airplane. CWT Rep. 292, Southern Calif. Cooperative Wind Tunnel, Mar. 20, 1953.

3. Runckel, Jack F., and Steinberg, Seymour: Effect of Leading-Edge Slats on the Aerodynamic Characteristics of a 45° Sweptback Wing-Fuselage Configuration at Mach Numbers of 0.4 to 1.03. NACA RM L53F23, 1953.

4. Arabian, Donald D., Runckel, Jack F., and Reid, Charles F., Jr.: Aerodynamic Load Measurements and Opening Characteristics of Automatic Leading-Edge Slats on a 45° Sweptback Wing at Transonic Speeds. NACA RM L53I30, 1953.

5. Ward, Vernon G., Whitcomb, Charles F., and Pearson, Merwin D.: Air-Flow and Power Characteristics of the Langley 16-Foot Transonic Tunnel With Slotted Test Section. NACA RM L52E01, 1952.

6. Osborne, Robert S.: High-Speed Wind-Tunnel Investigation of the Longitudinal Stability and Control Characteristics of a 1/16-Scale Model of the D-558-2 Research Airplane at High Subsonic Mach Numbers and at a Mach Number of 1.2. NACA RM L9C04, 1949.

7. Ritchie, Virgil S., and Pearson, Albin O.: Calibration of the Slotted Test Section of the Langley 8-Foot Transonic Tunnel and Preliminary Experimental Investigation of Boundary-Reflected Disturbances. NACA RM L51K14, 1952.

8. Solomon, William, and Schmeer, James W.: Effect of Longitudinal Wing Position on the Pressure Characteristics at Transonic Speeds of a 45° Sweptback Wing-Fuselage Model. NACA RM L52K05a, 1953.

9. West, F. E., Jr., and Henderson, James H.: Relationship of Flow Over a 45° Sweptback Wing With and Without Leading-Edge Chord-Extensions to Longitudinal Stability Characteristics at Mach Numbers From 0.60 to 1.03. NACA RM L53H18b, 1953.

TABLE I.- DIMENSIONS OF THE MODEL

Wing geometry:	
Root and tip airfoil section (parallel to plane of symmetry)	NACA $64_{(06)}$A007
Area, sq ft	8.46
Span, in.	65.84
Mean aerodynamic chord, in.	20.39
Location of pitching-moment axis, percent $\bar{c}$	35.0
Root chord, in. (parallel to plane of symmetry)	28.55
Tip chord, in. (parallel to plane of symmetry)	8.57
Taper ratio	0.30
Aspect ratio	3.56
Sweep angle, deg (25-percent-chord line)	45.0
Incidence, deg	0
Dihedral, deg	0
Geometric twist, deg	0
Leading-edge slats:	
Chord (percent of local wing chord)	20
Span (percent of wing semispan)	
0.35b/2 to 0.95b/2 configuration	60
0.46b/2 to 0.95b/2 configuration	49
Deflection, deg	10
Gap (percent slat chord)	19
Extension (percent slat chord)	45
Horizontal tail:	
Root and tip airfoil sections (parallel to plane of symmetry)	NACA $64_{(06)}$A007
Area, sq ft (including area covered by fuselage)	2.23
Span, in.	33.80
Mean aerodynamic chord, in.	10.46
Root chord, in.	14.65
Tip chord, in.	4.39
Taper ratio	0.30
Aspect ratio	3.56
Sweep angle, deg (25-percent-chord line)	45.0
Dihedral, deg	0
Tail length, in. (wing c/4 to tail c/4; $\delta_H = 0^o$)	26.74
Ratio of horizontal tail area to wing area	0.263
Tail height, fraction of tail length below wing chord plane extended	0.03
Rotation point of horizontal tail, fraction of tail chord	0.77

TABLE I.- DIMENSIONS OF THE MODEL - CONCLUDED

Vertical tail:	
Root and tip airfoil sections (parallel to fuselage reference line)	NACA $64_{(06)}$A007
Area, sq ft (excluding dorsal fin)	0.90
Span, in. (unblanketed)	13.43
Mean aerodynamic chord, in.	9.91
Root chord, in.	13.87
Tip chord, in.	4.18
Taper ratio	0.30
Aspect ratio	1.49
Sweep angle, deg (25-percent-chord line)	45.0
Fuselage:	
Length, in. (including faired nose)	88.56
Depth, maximum, in. (over canopy)	11.48
Width, maximum, in.	10.05

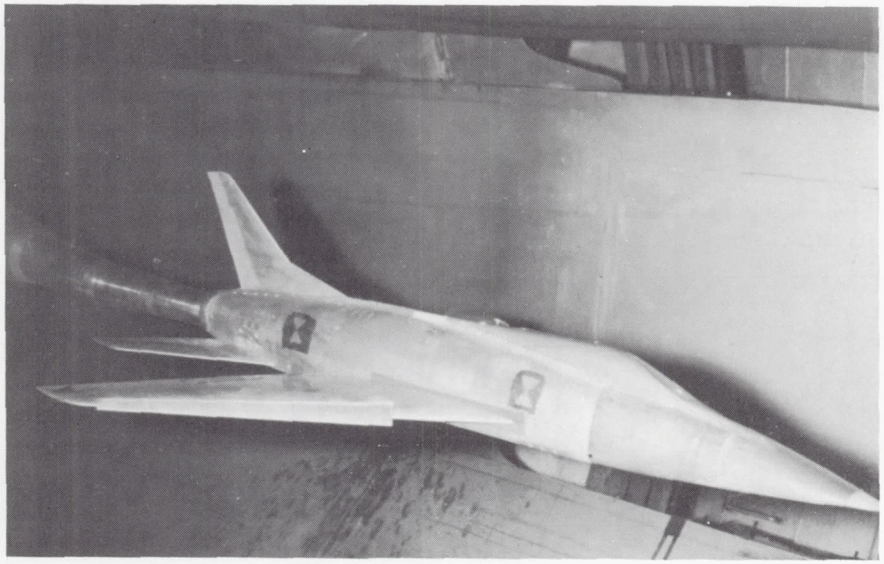

L-76667

(a) Complete model with 35-to-95-percent b/2 slats extended.

Figure 1.- Photograph of the fighter-type model in the Langley 16-foot transonic tunnel.

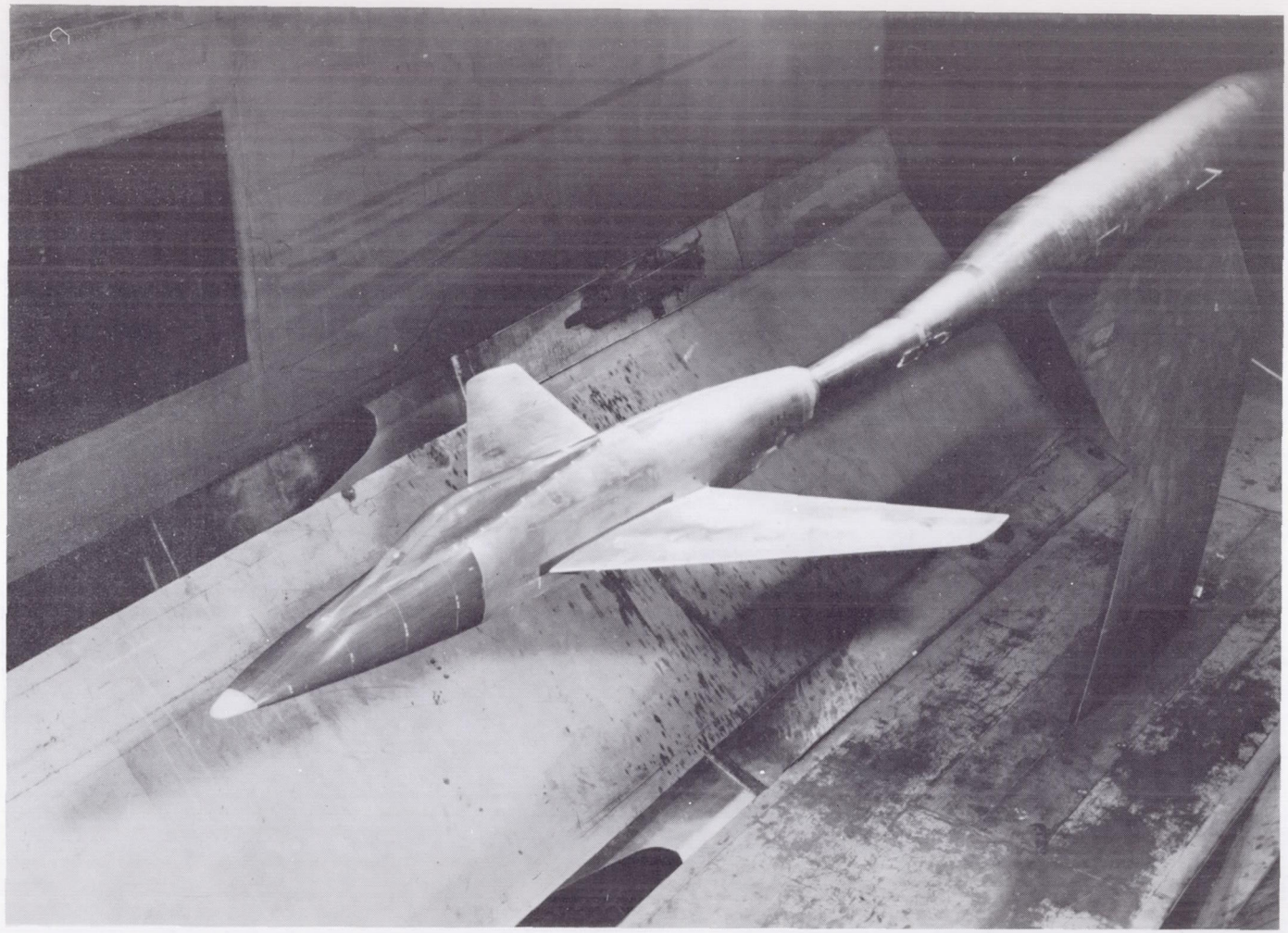

L-76464

(b) Tail-off configuration with slats retracted.

Figure 1.- Concluded.

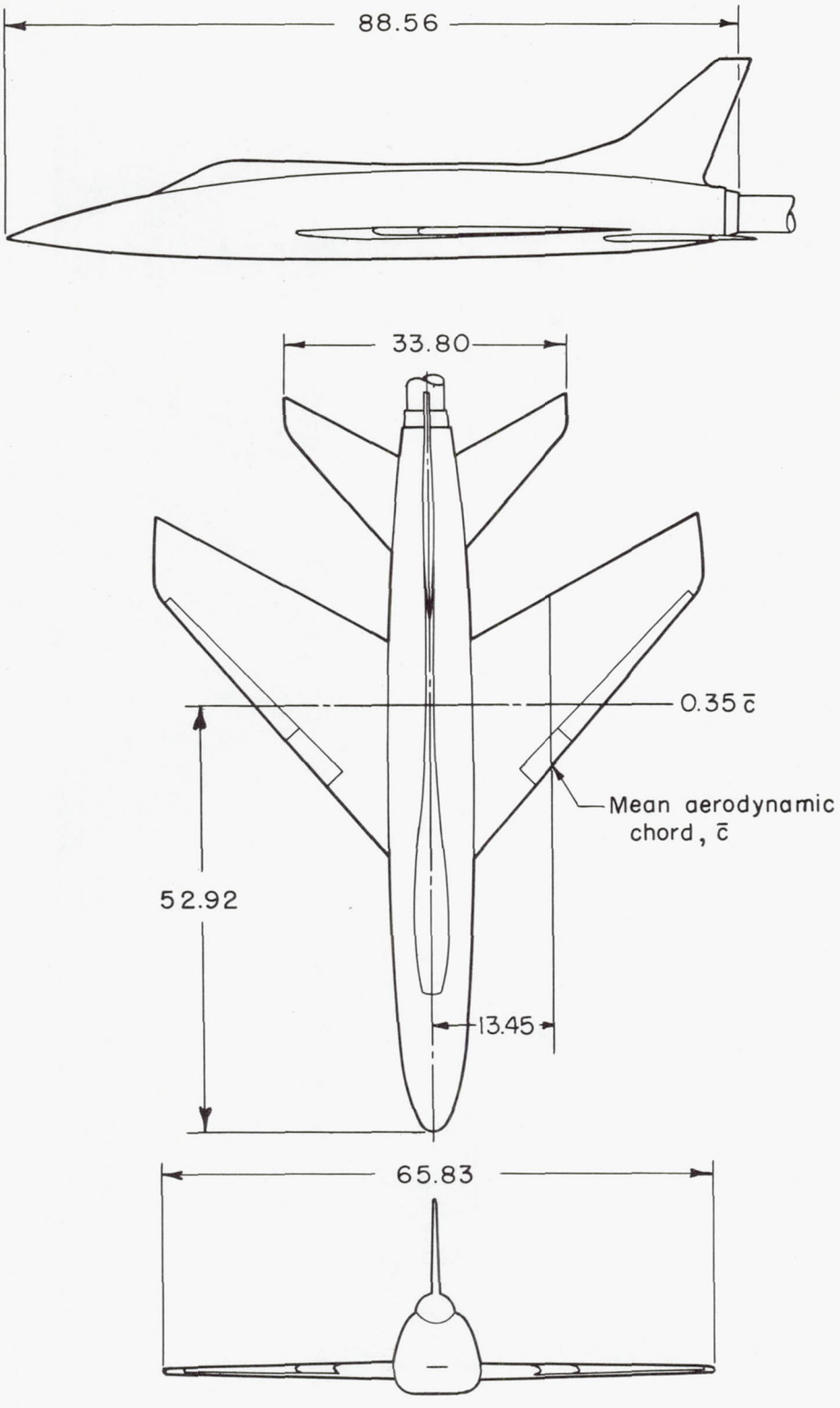

Figure 2.- Three-view drawing of the model with slats retracted. All dimensions are in inches. See table I for other dimensions.

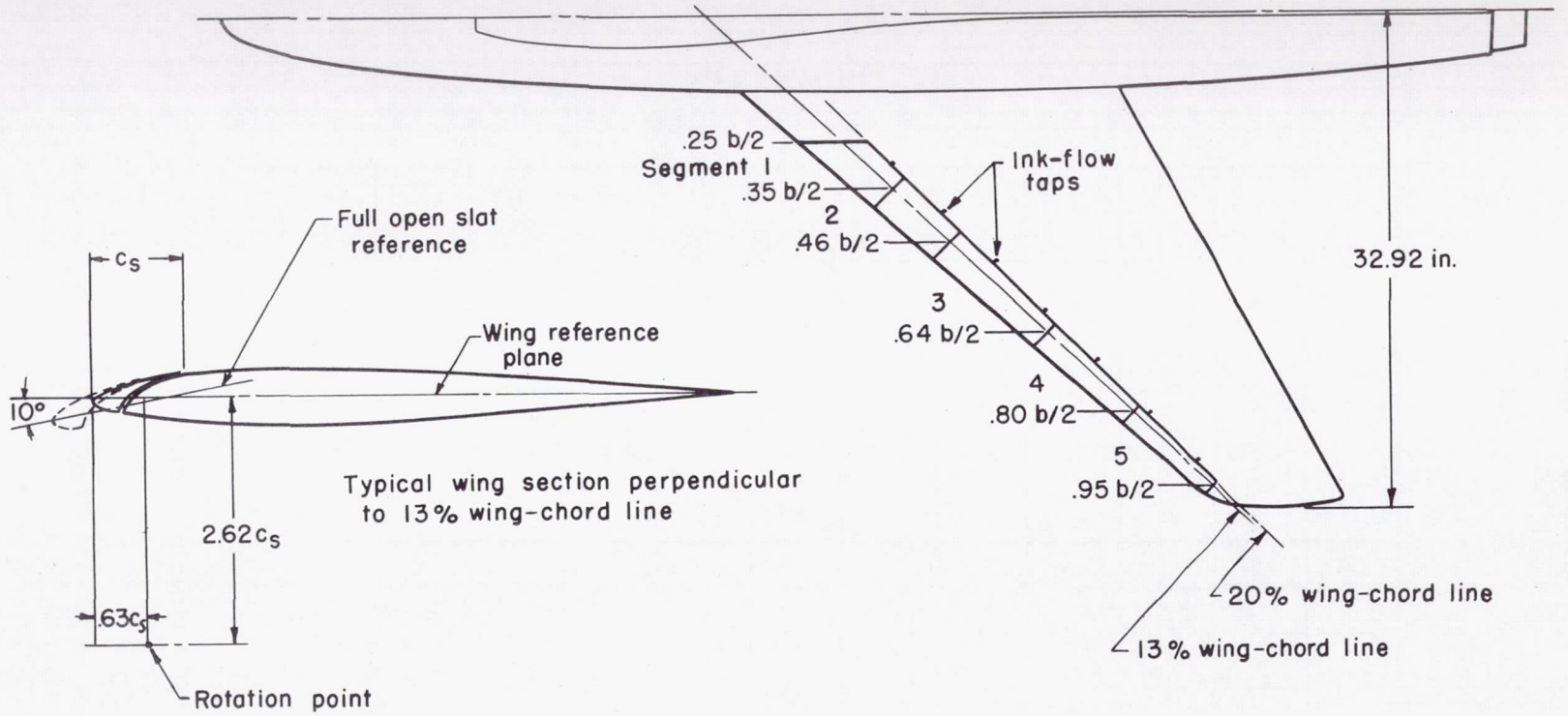

Ink-flow taps located at 22% chord line and at
20%, 30%, 40%, 50%, 60%, 70%, 80% and 90% b/2

Figure 3.- Detail of slat segments and location of ink-flow orificies.

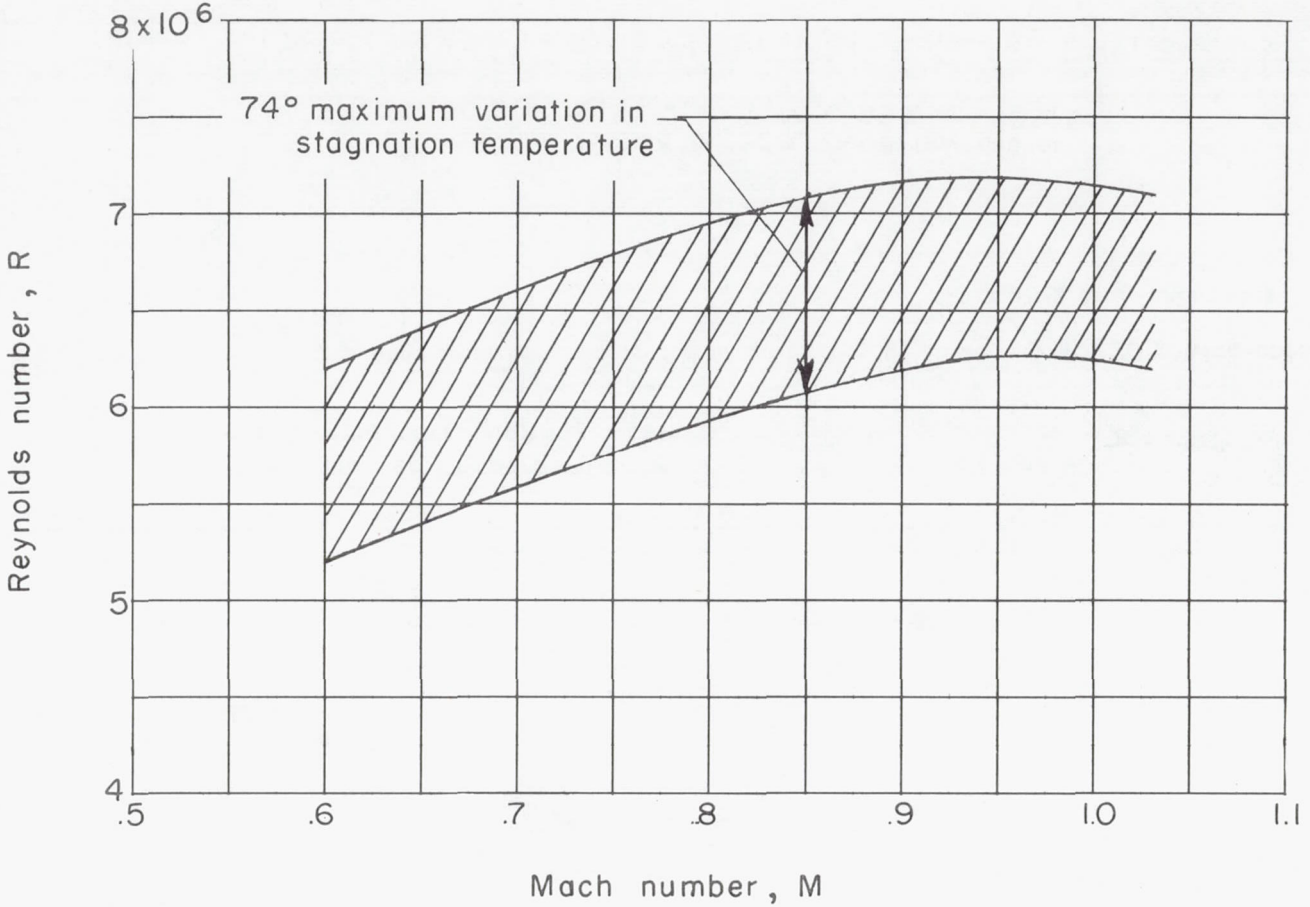

Figure 4.- Variation with Mach number of Reynolds number based on $\bar{c}$ = 1.699 feet.

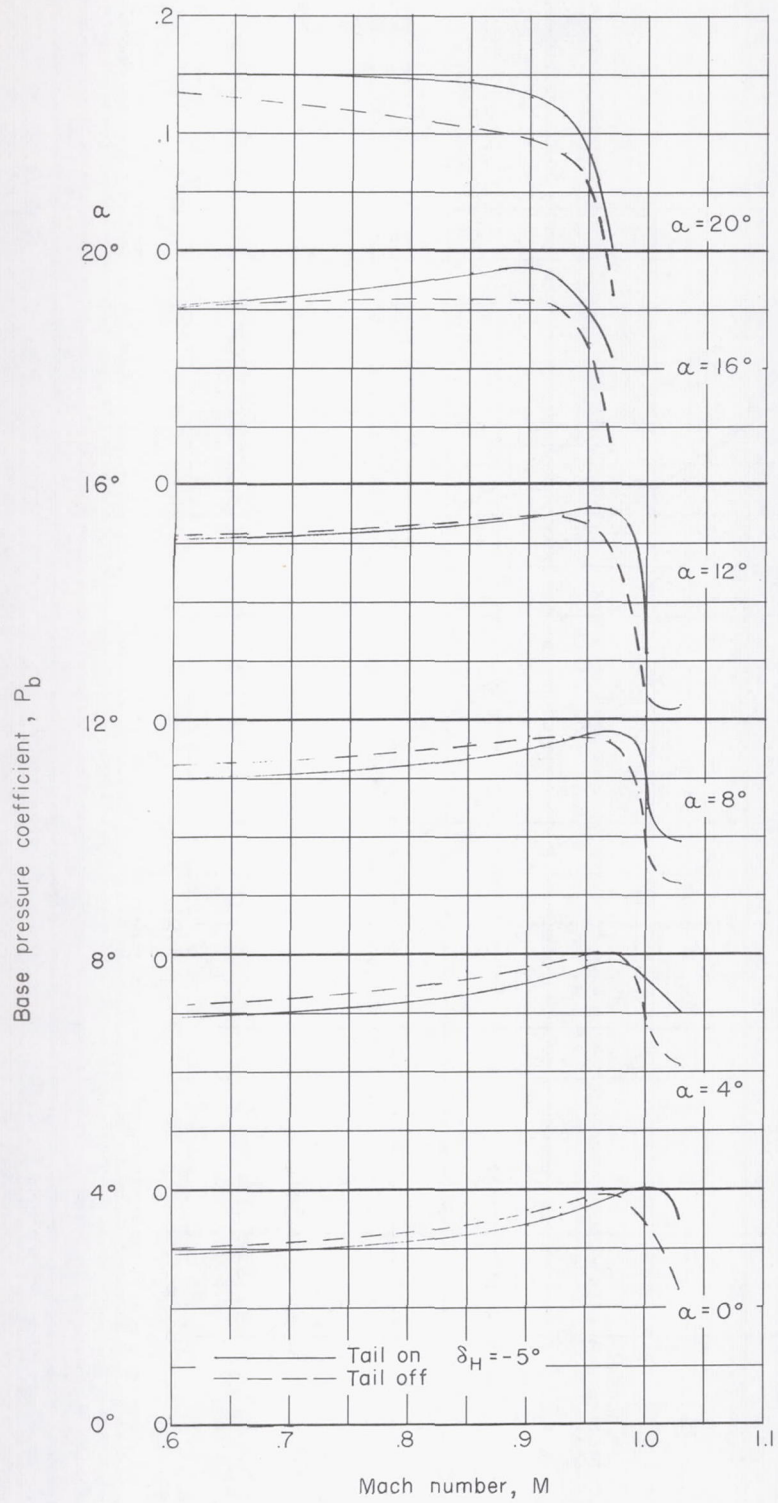

Figure 5.- Effect of Mach number on the base pressure coefficient for the complete model and for a tail-off configuration. Slats retracted.

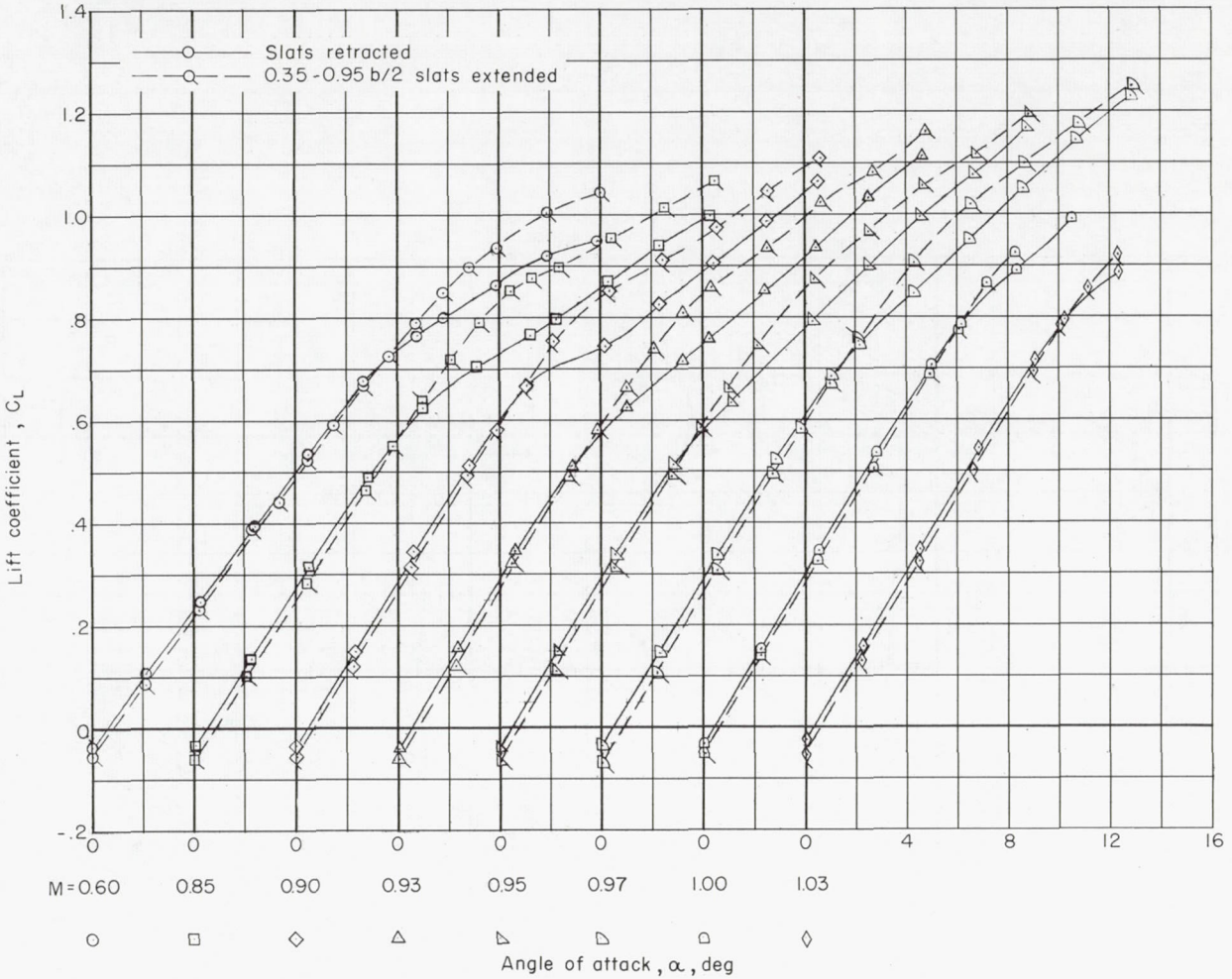

(a) Slats retracted and 0.35b/2 slats extended.

Figure 6.- Variation with angle of attack of lift coefficient for the complete model. $\delta_H = -5^\circ$.

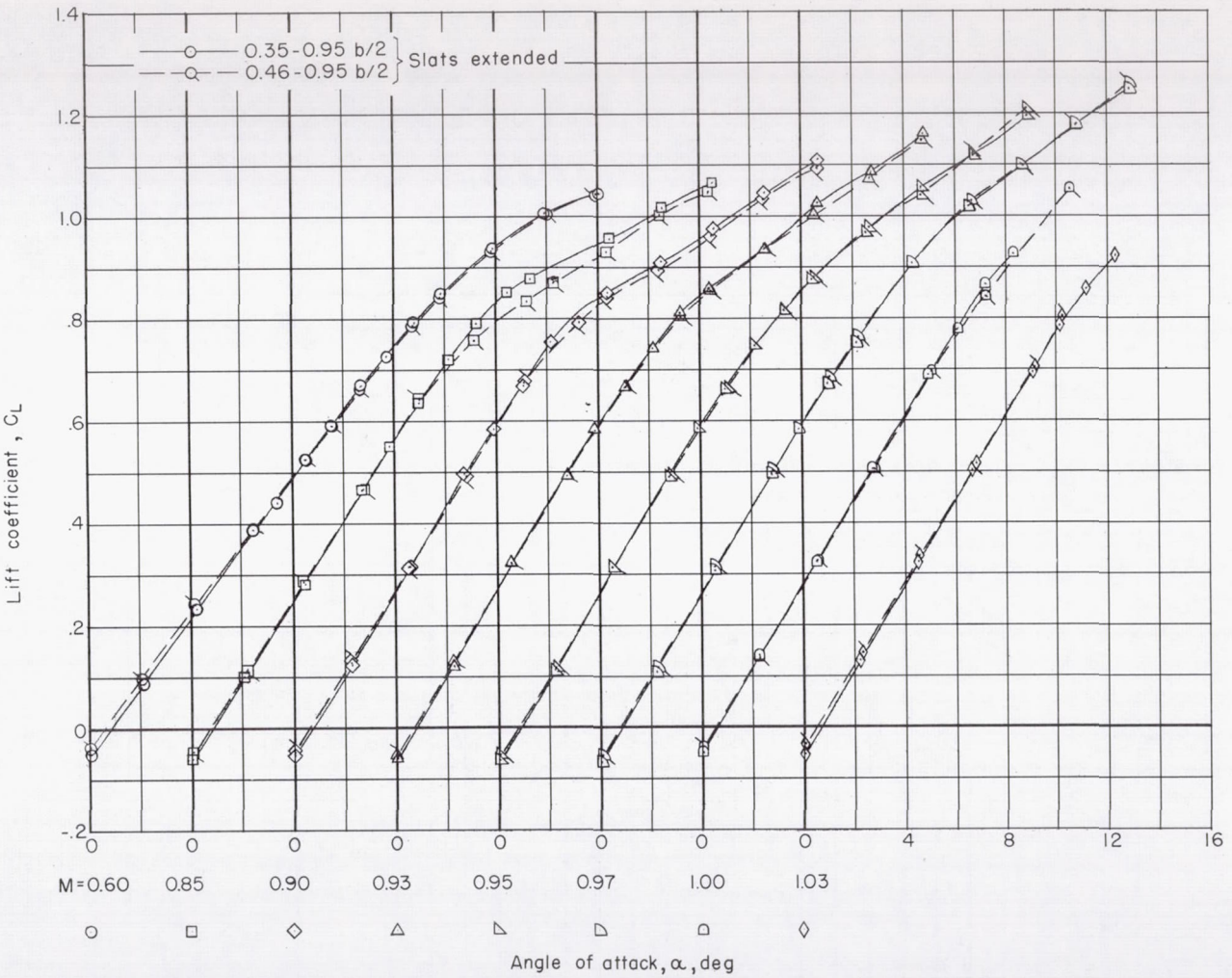

(b) 0.35b/2 to 0.95b/2 and 0.46b/2 to 0.95b/2 slats extended.

Figure 6.- Concluded.

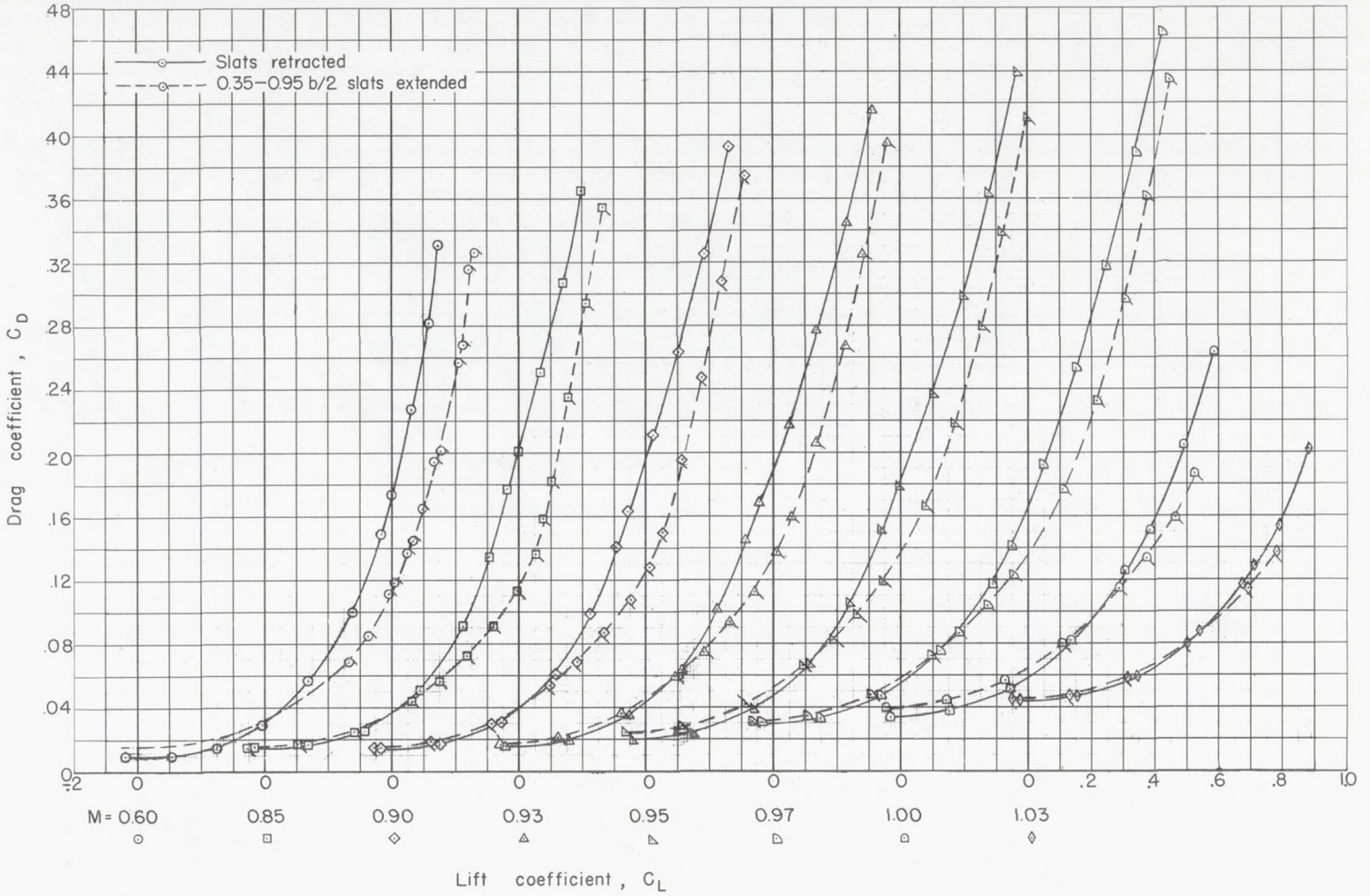

(a) Slats retracted and 0.35b/2 to 0.95b/2 slats extended.

Figure 7.- Variation with lift coefficient of the drag coefficient for the complete model. $\delta_H = -5^\circ$.

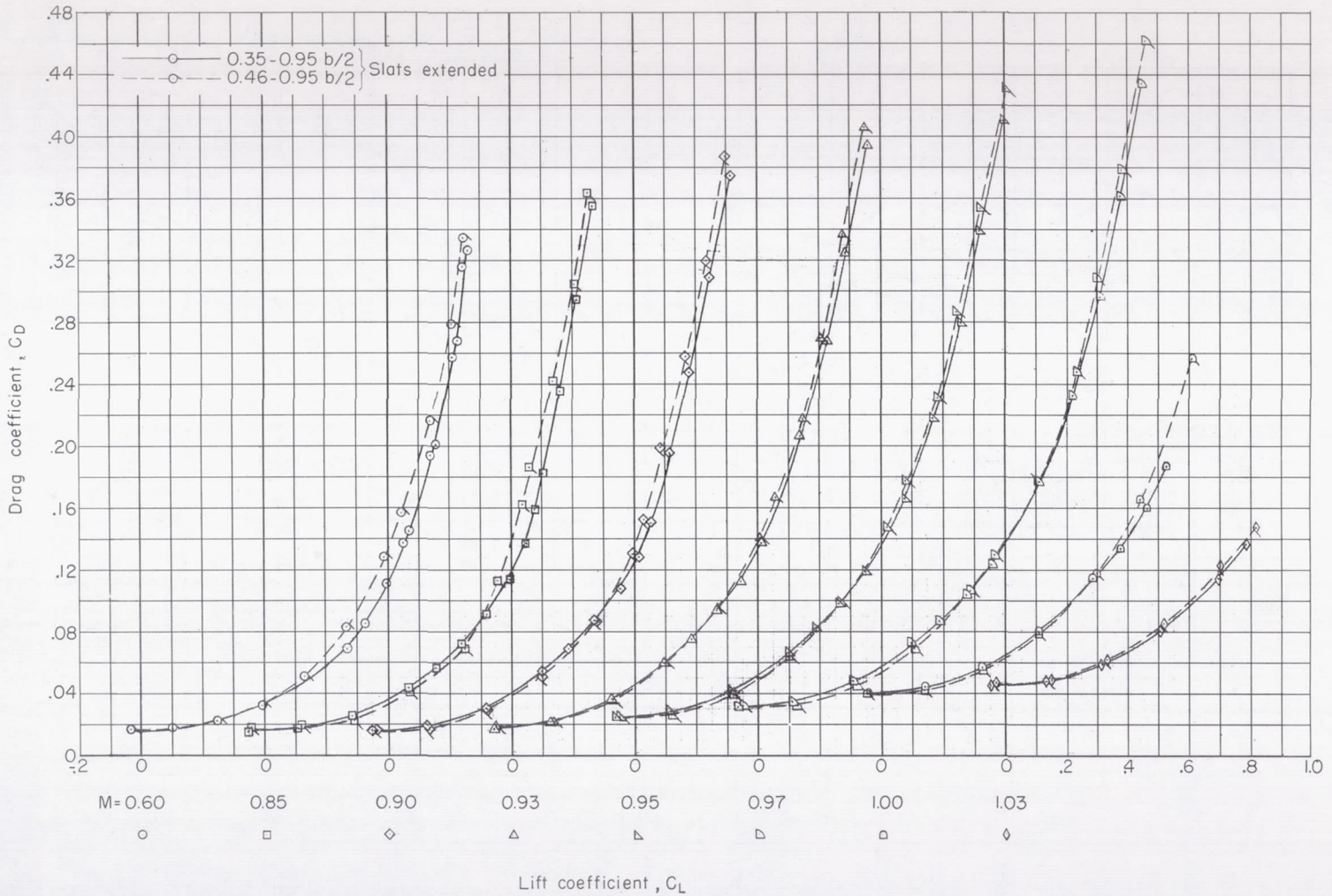

(b) 0.35b/2 to 0.95b/2 and 0.46b/2 to 0.95b/2 slats extended.

Figure 7.- Concluded.

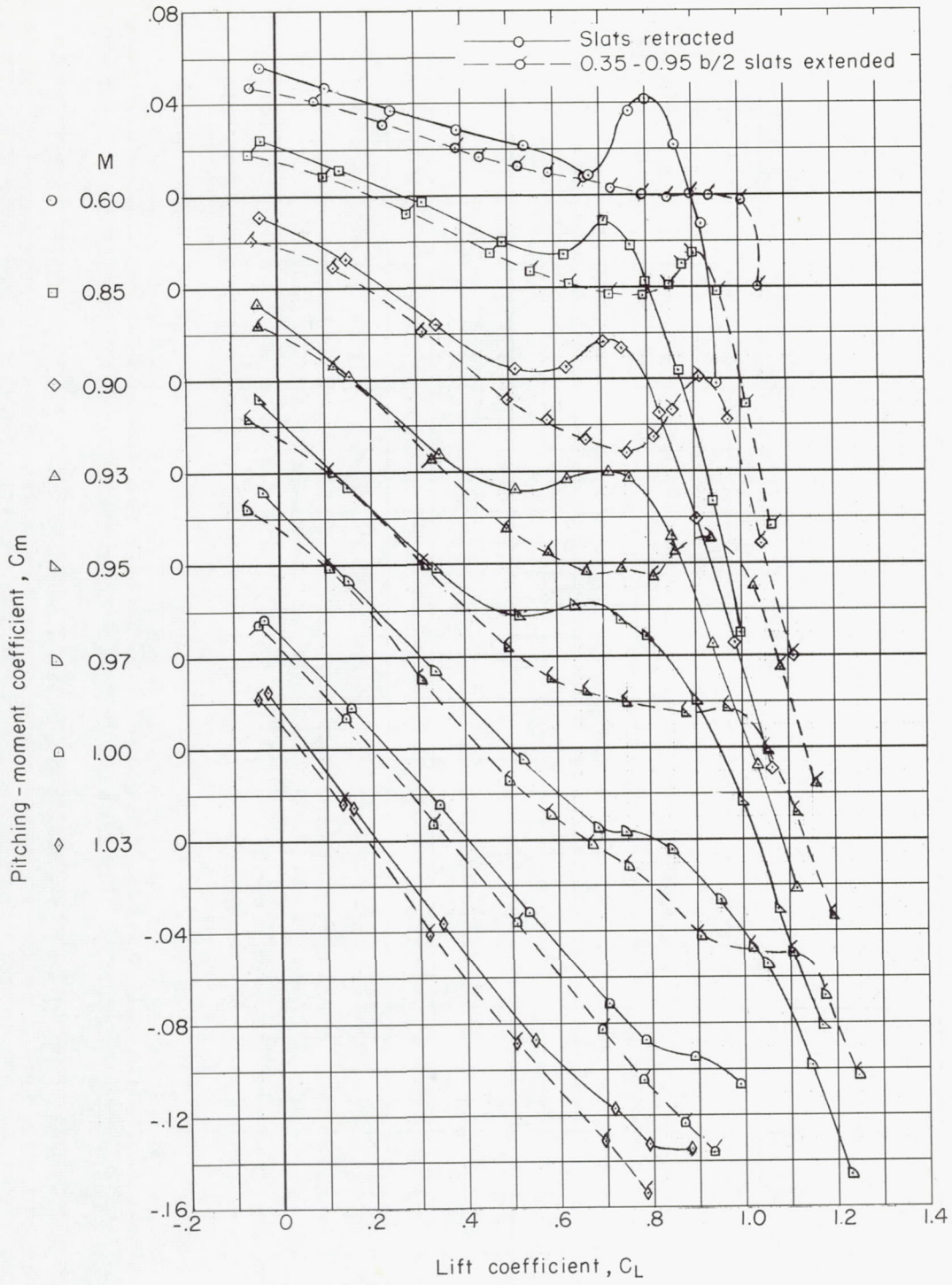

(a) Slats retracted and 0.35b/2 to 0.95b/2 slats extended.

Figure 8.- Variation with lift coefficient of the pitching-moment coefficient for the complete model. $\delta_H = -5^\circ$.

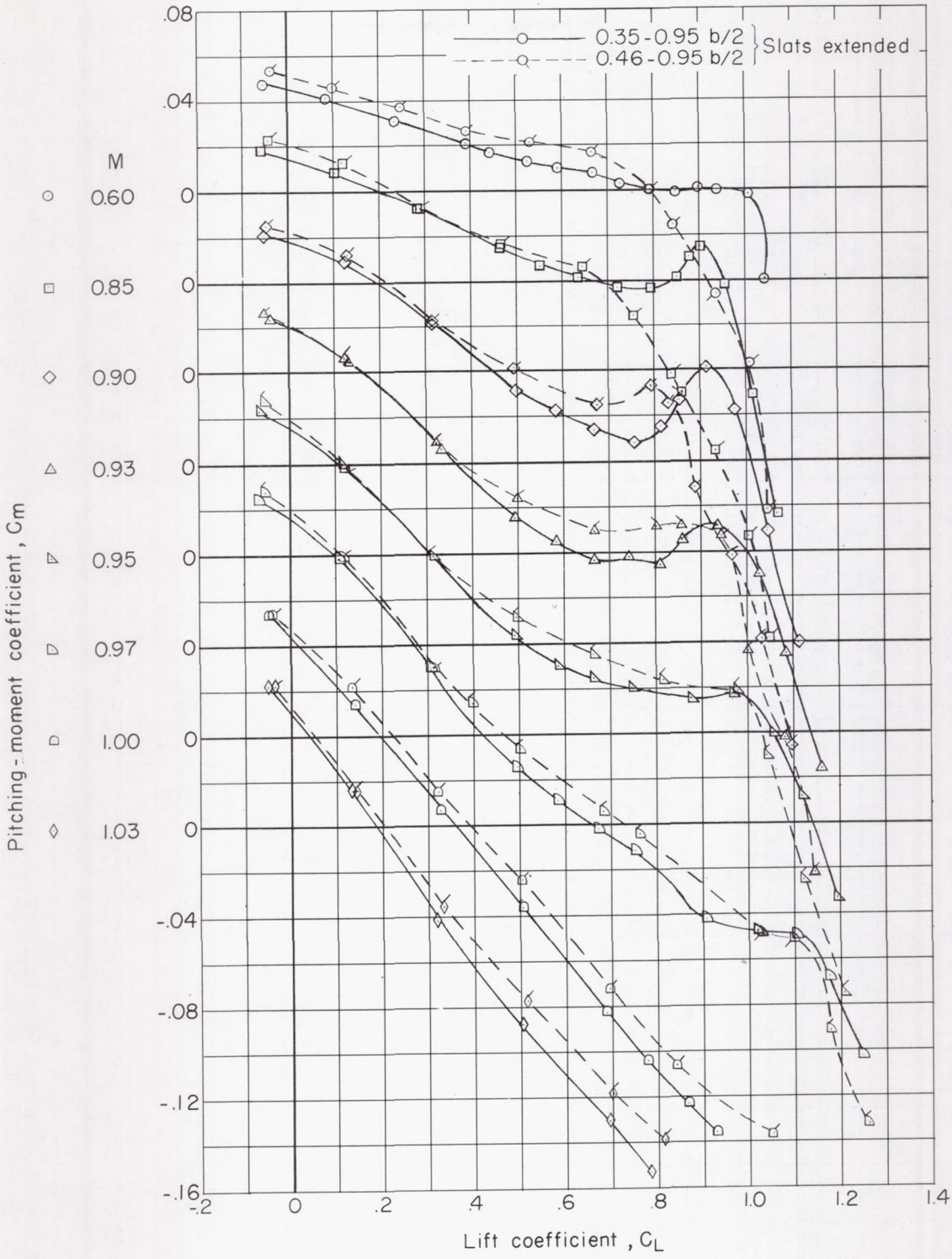

(b) 0.35b/2 to 0.95b/2 and 0.46b/2 to 0.95b/2 slats extended.

Figure 8.- Concluded.

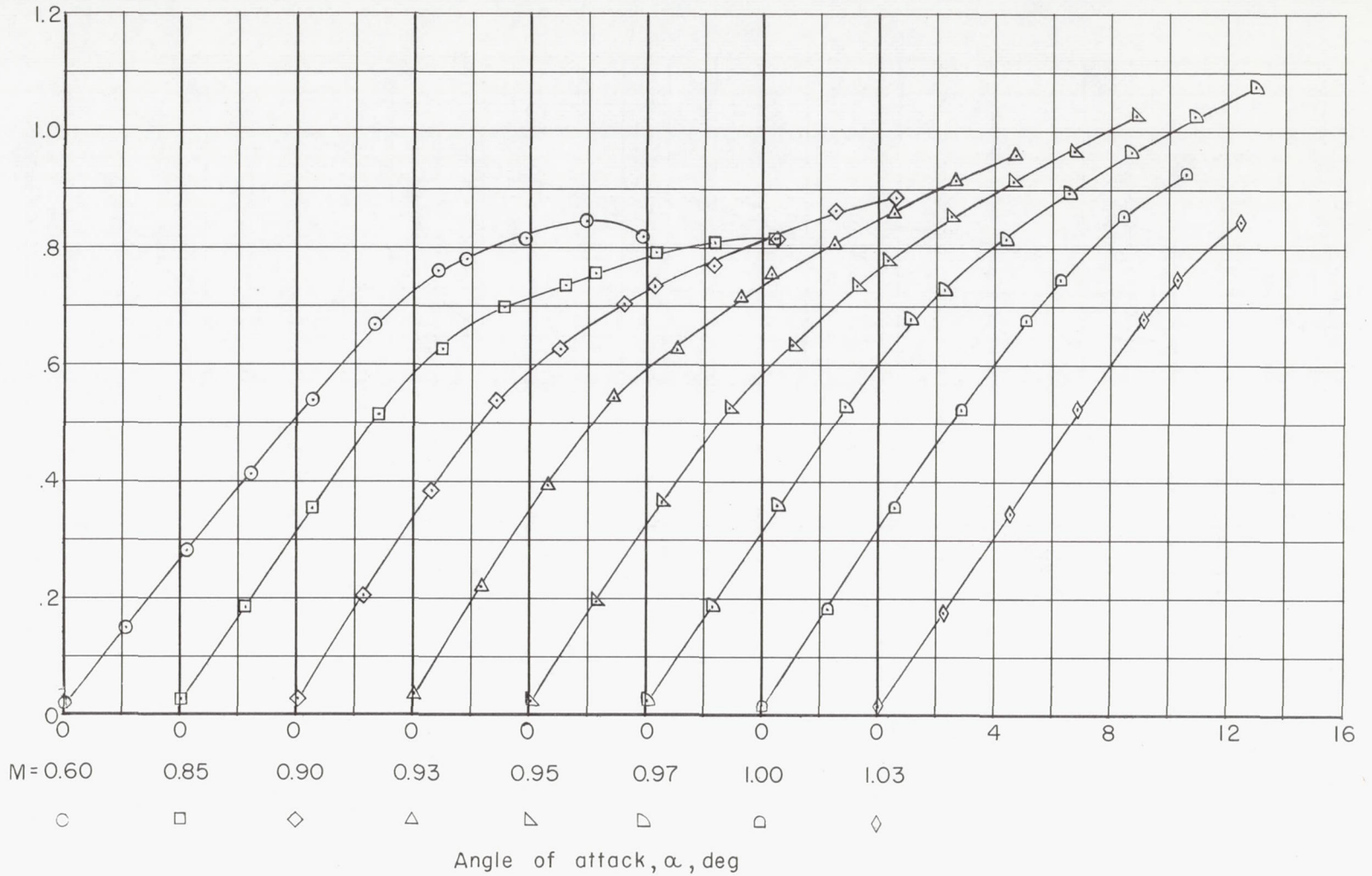

(a) Slats retracted.

Figure 9.- Variation with angle of attack of lift coefficient for tail-off configuration.

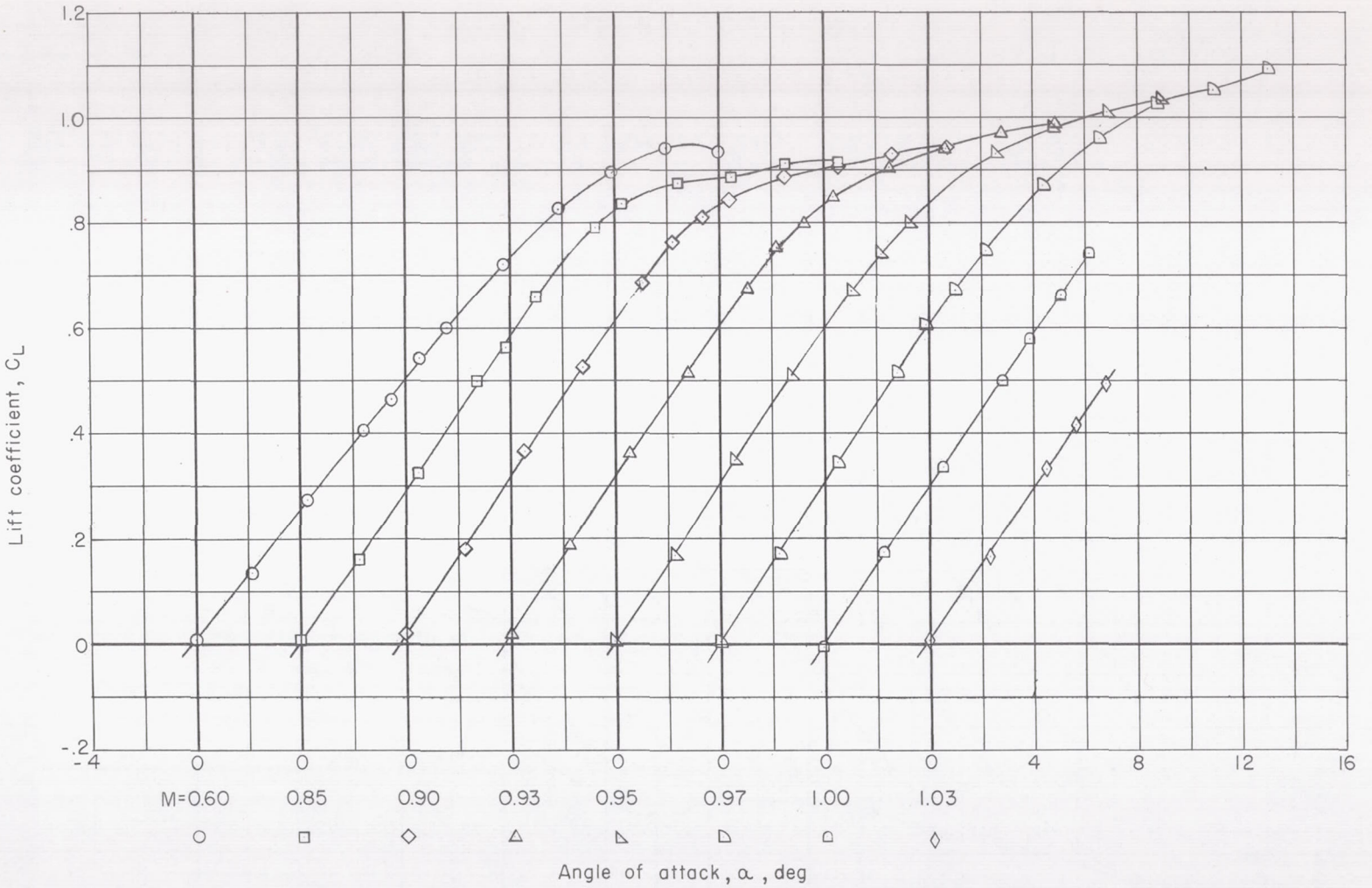

(b) 0.35b/2 to 0.95b/2 slats extended.

Figure 9.- Continued.

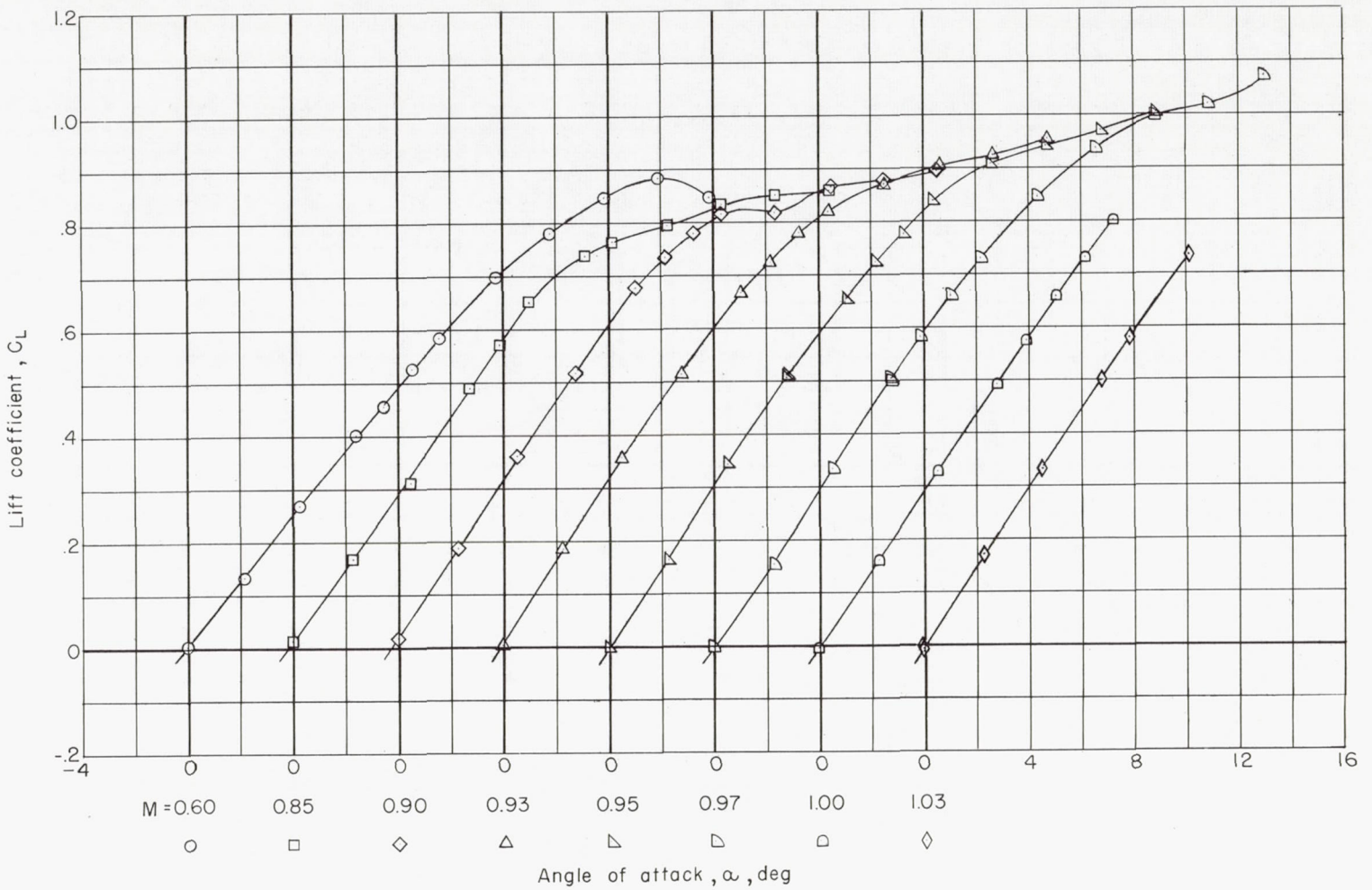

(c) 0.46b/2 to 0.95b/2 slats extended.

Figure 9.- Concluded.

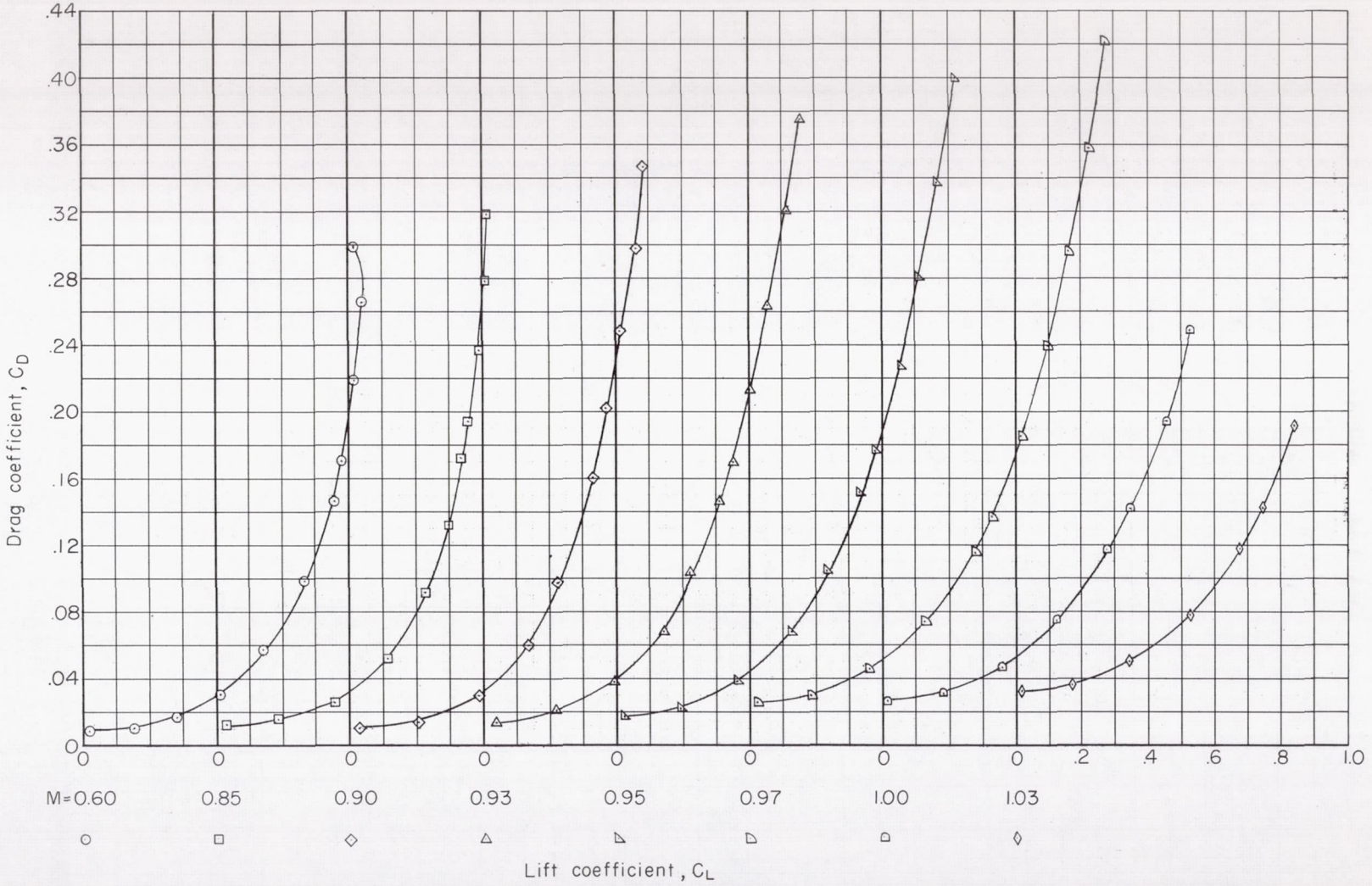

(a) Slats retracted.

Figure 10.- Variation with lift coefficient of drag coefficient for tail-off configurations.

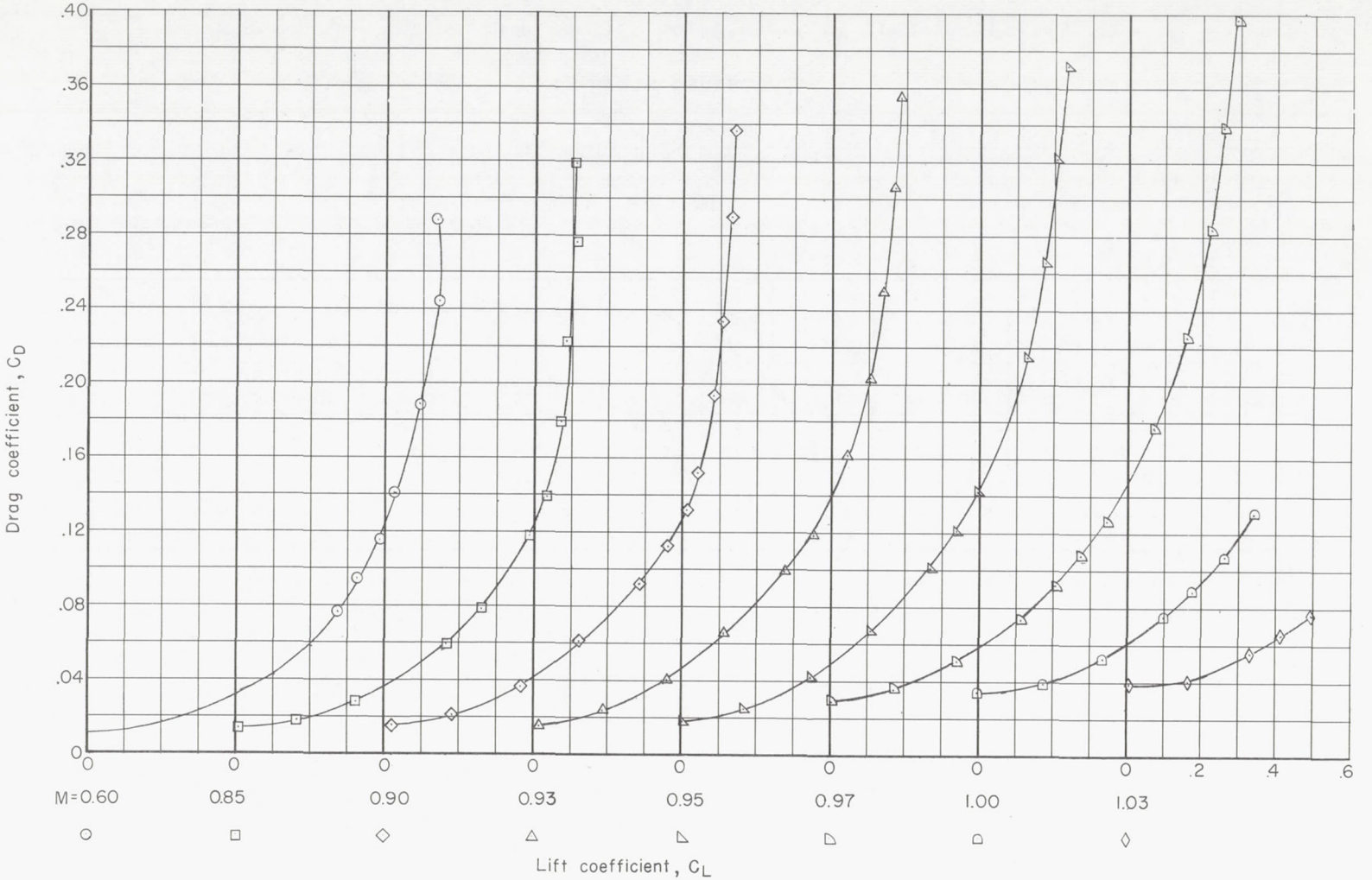

(b) 0.35b/2 to 0.95b/2 slats extended.

Figure 10.- Continued.

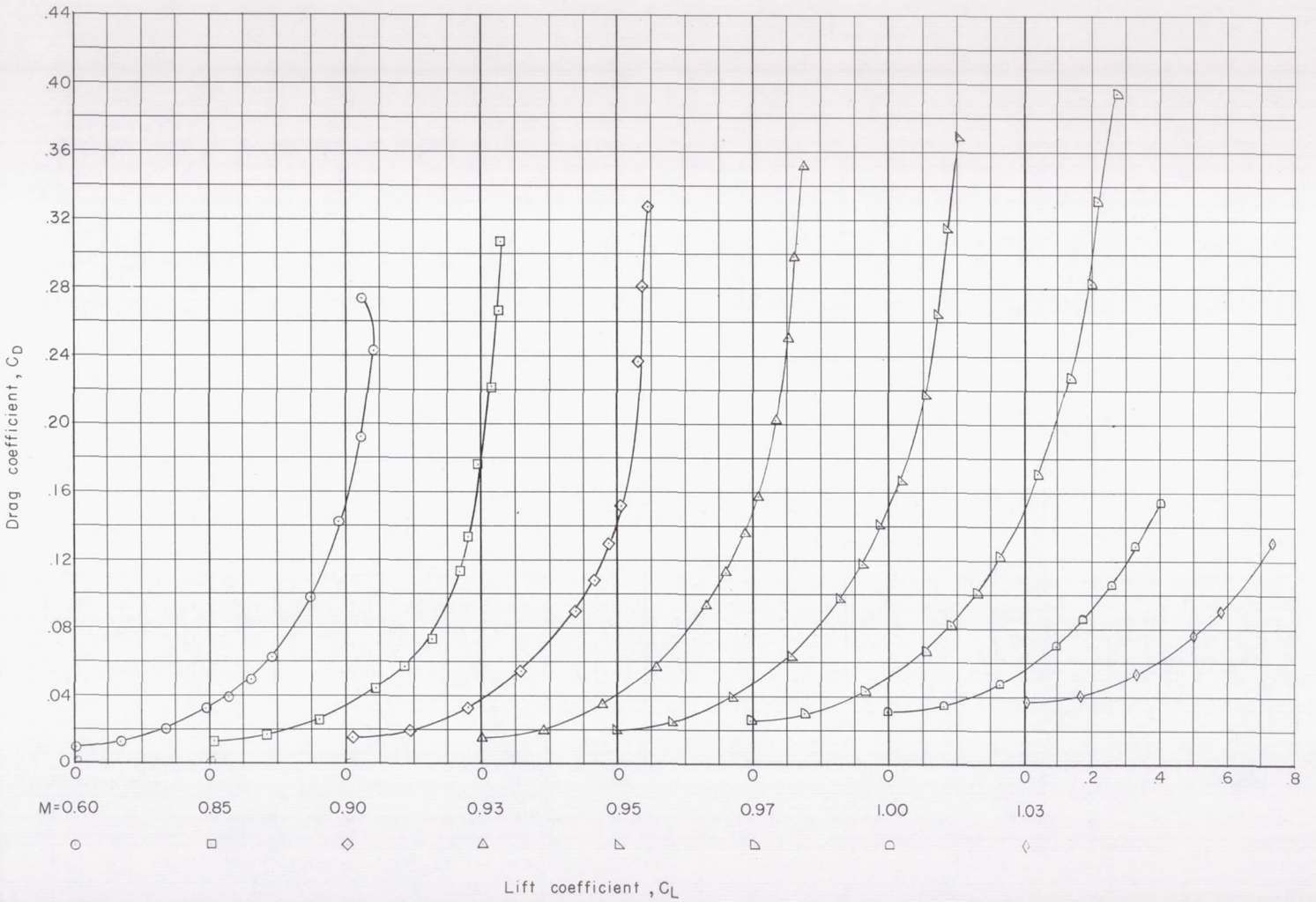

(c) 0.46b/2 to 0.95b/2 slats extended.

Figure 10.- Concluded.

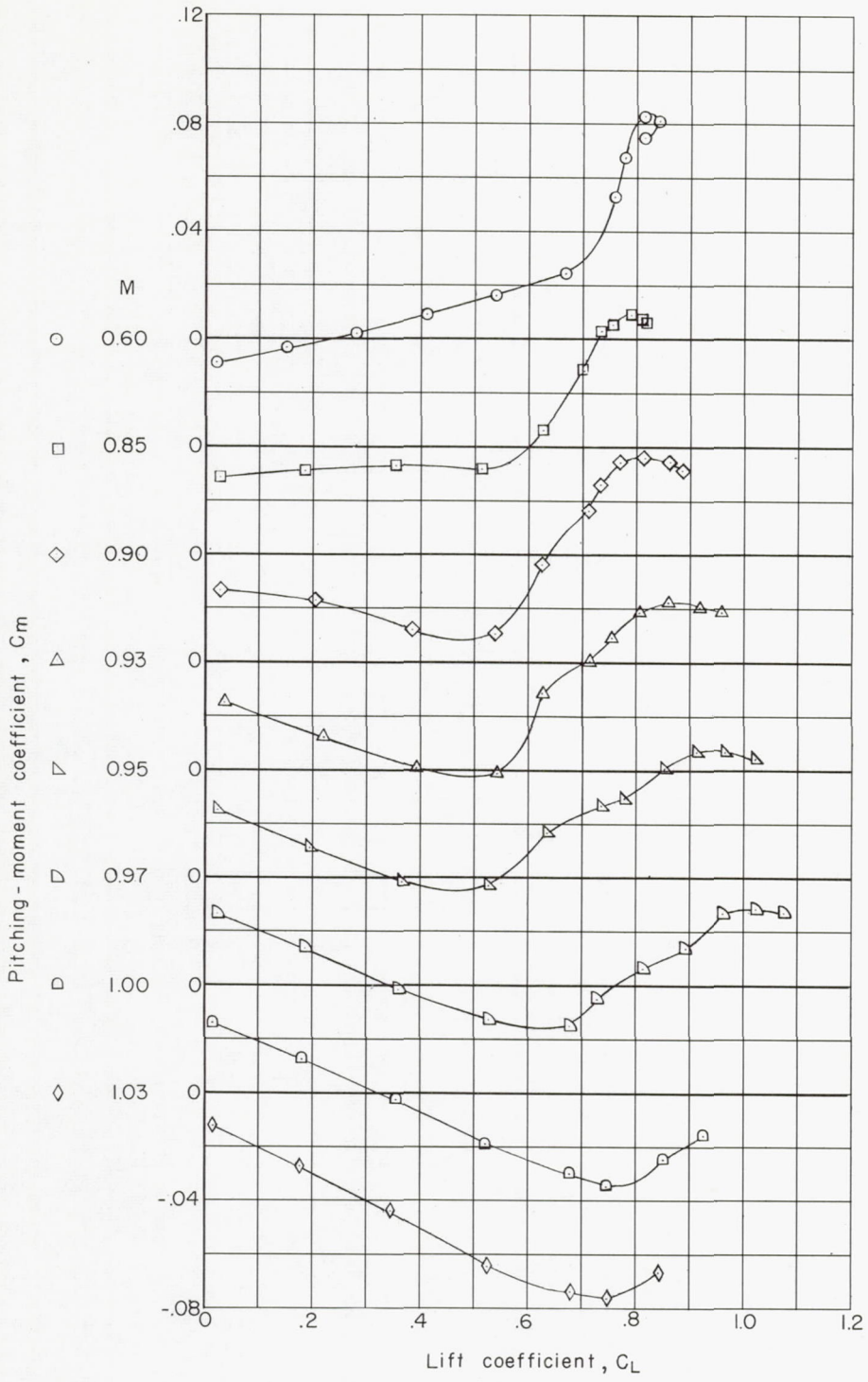

(a) Slats retracted.

Figure 11.- Variation with lift coefficient of pitching-moment coefficient for tail-off configurations.

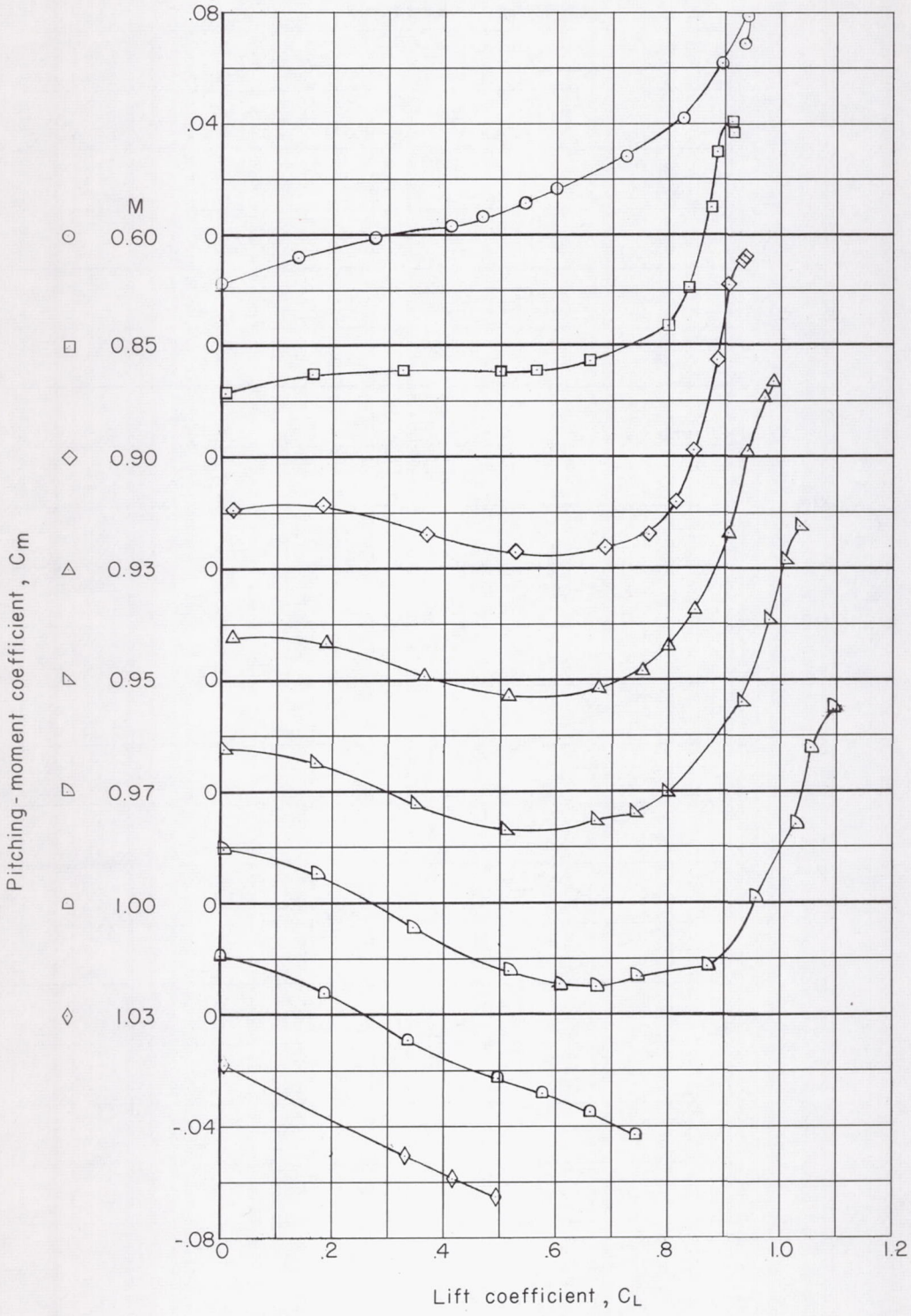

(b) 0.35b/2 to 0.95b/2 slats extended.

Figure 11.- Continued.

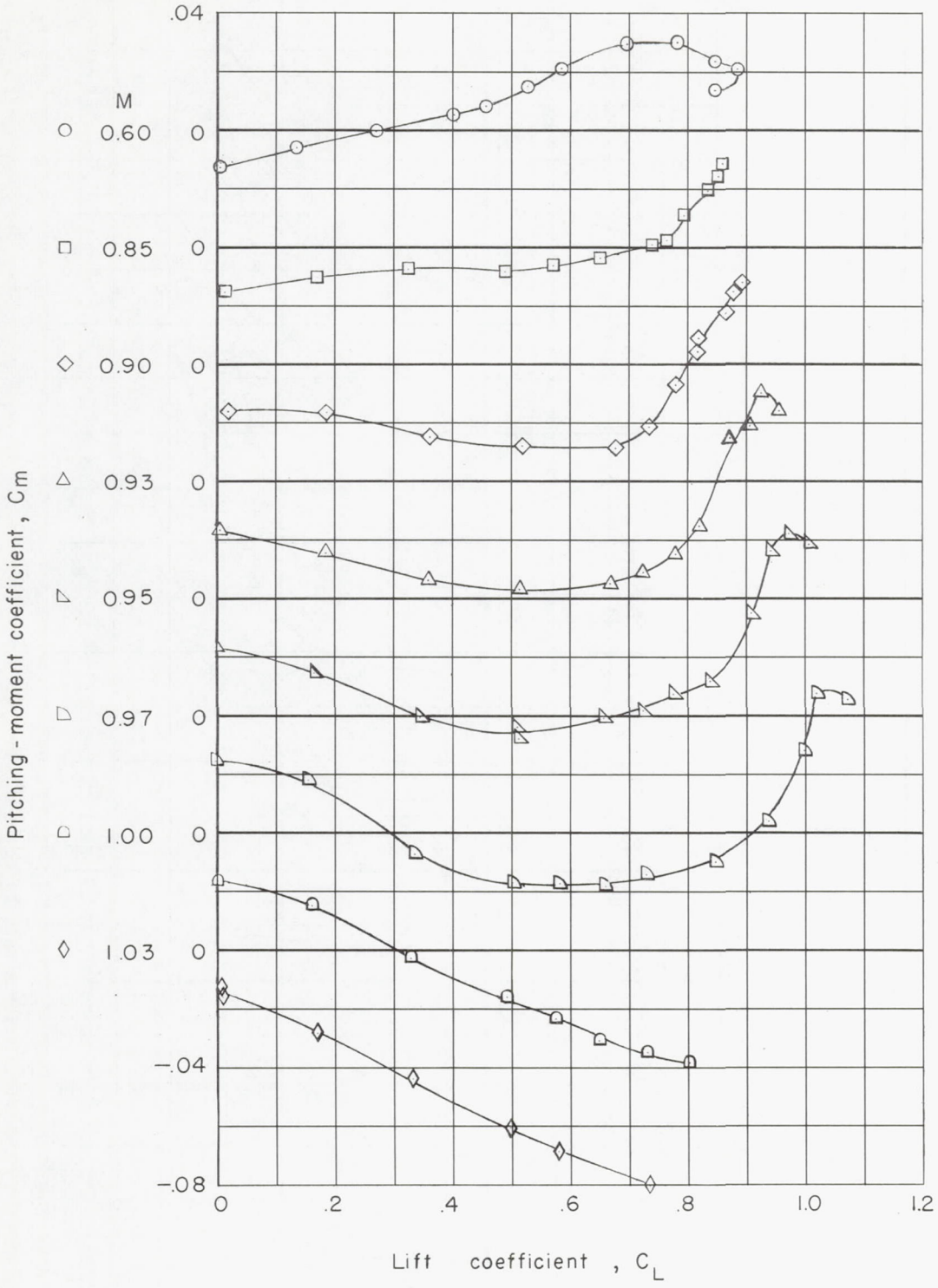

(c) 0.46b/2 to 0.95b/2 slats extended.

Figure 11.- Concluded.

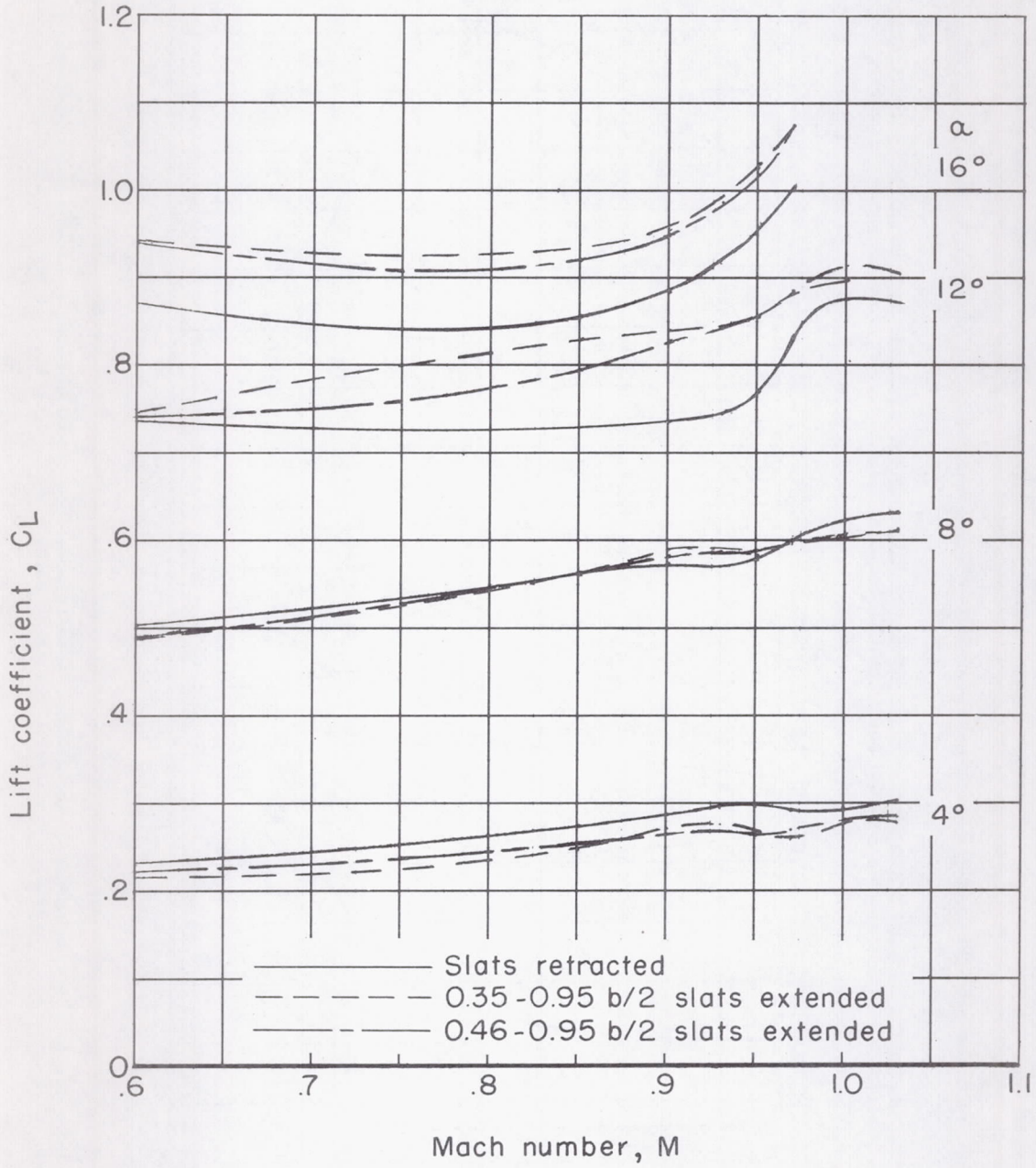

Figure 12.- Effect of Mach number on lift coefficient for the complete model. $\delta_H = -5^\circ$.

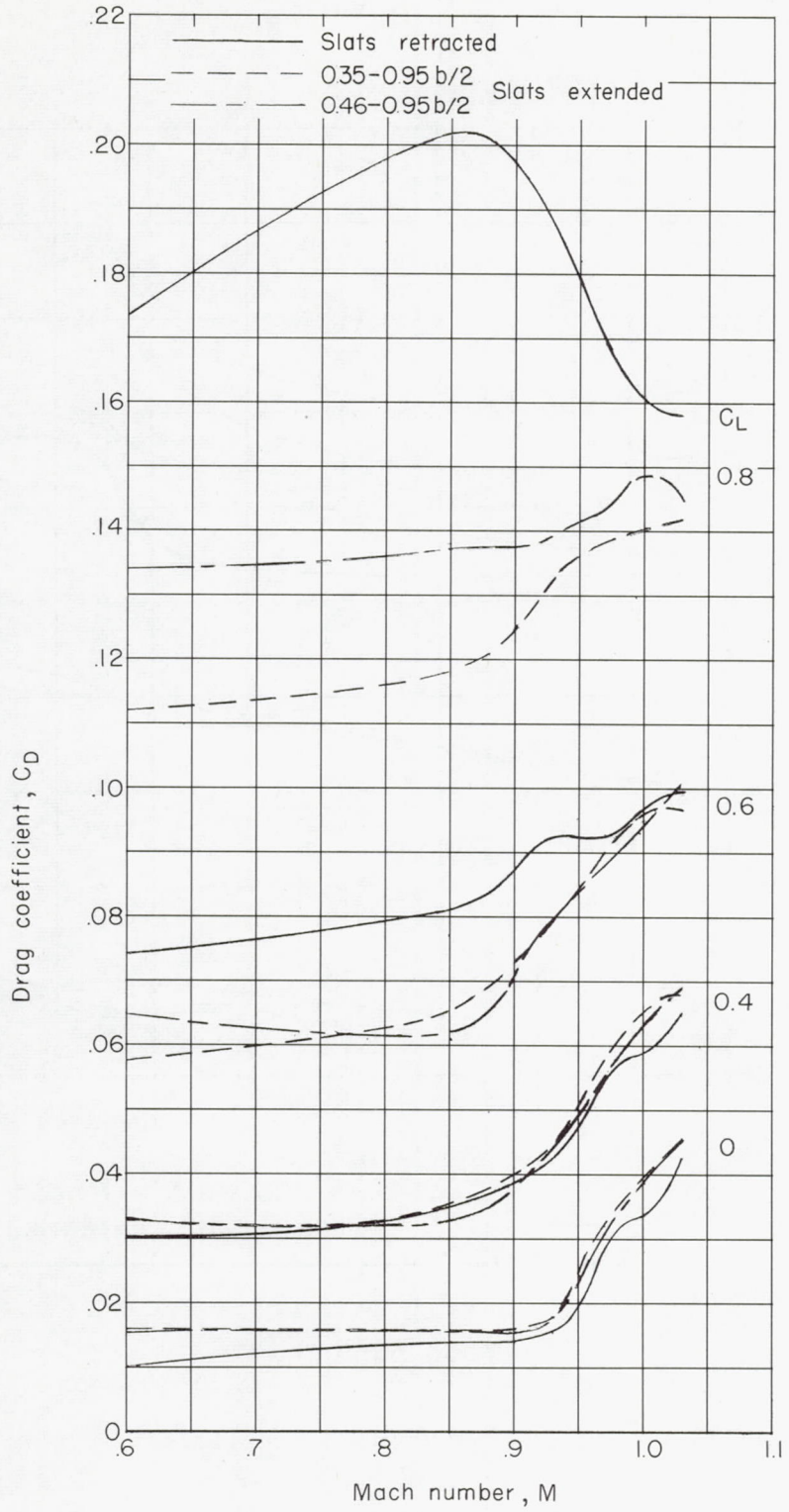

Figure 13.- Effect of Mach number on drag coefficient for the complete model at several lift coefficients. $\delta_H = -5^\circ$.

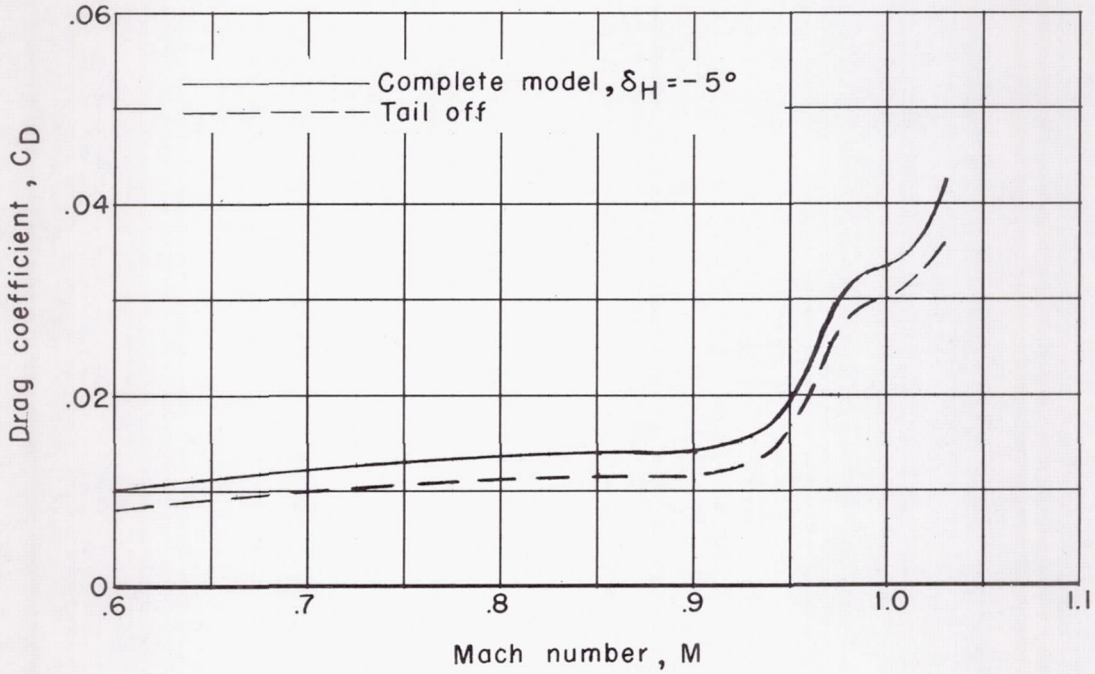

Figure 14.- Effect of Mach number on drag coefficient at zero lift for a complete model and a tail-off configuration. Slats retracted.

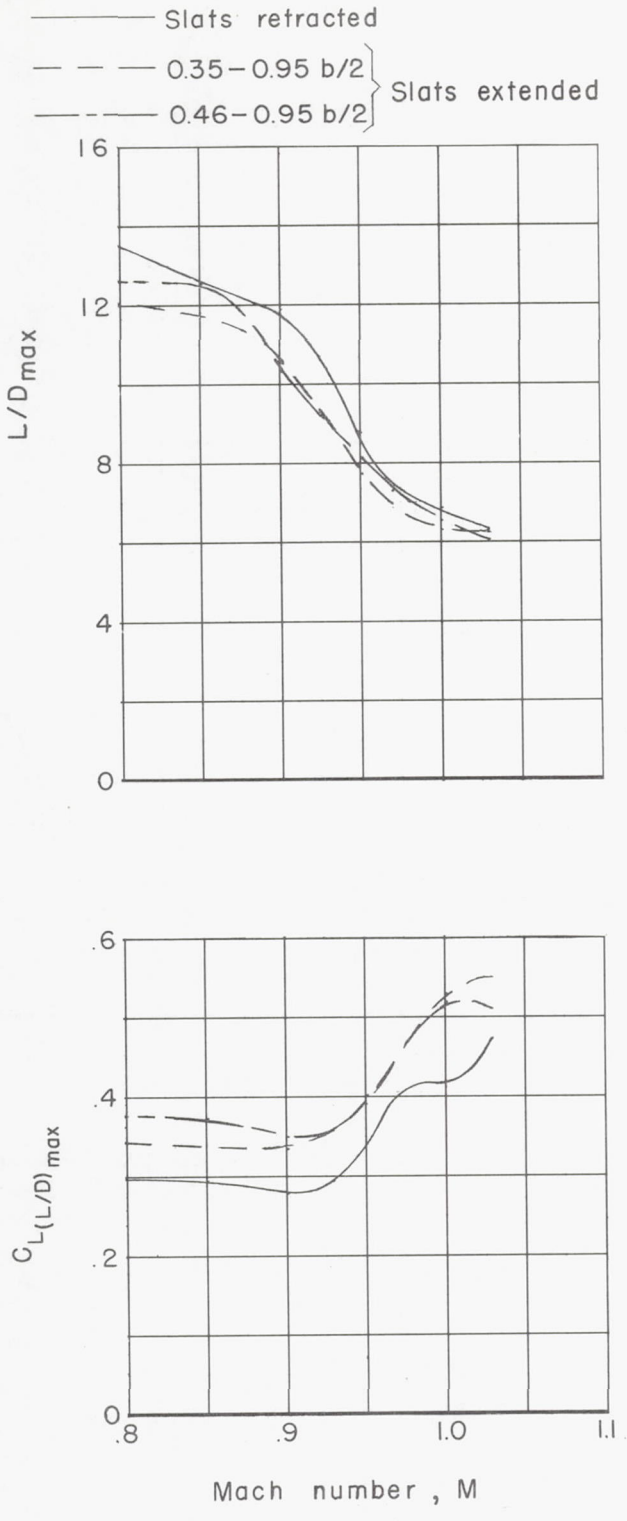

Figure 15.- Effect of Mach number on L/D_{max} and lift coefficient for L/D_{max}. Complete model. $\delta_H = -5^\circ$.

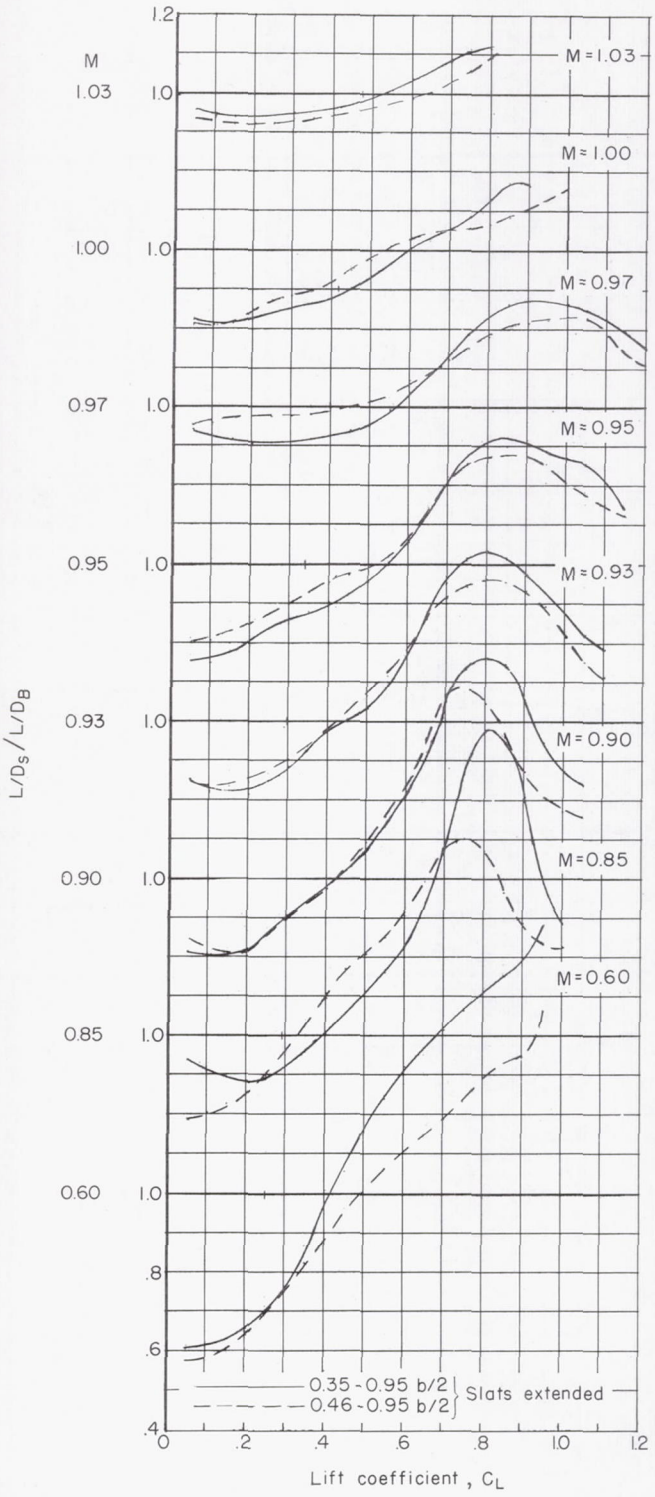

Figure 16.- Variation with lift coefficient of the ratio of L/D for configurations with slats extended to L/D for the model with slats retracted. Complete model. $\delta_H = -5^\circ$.

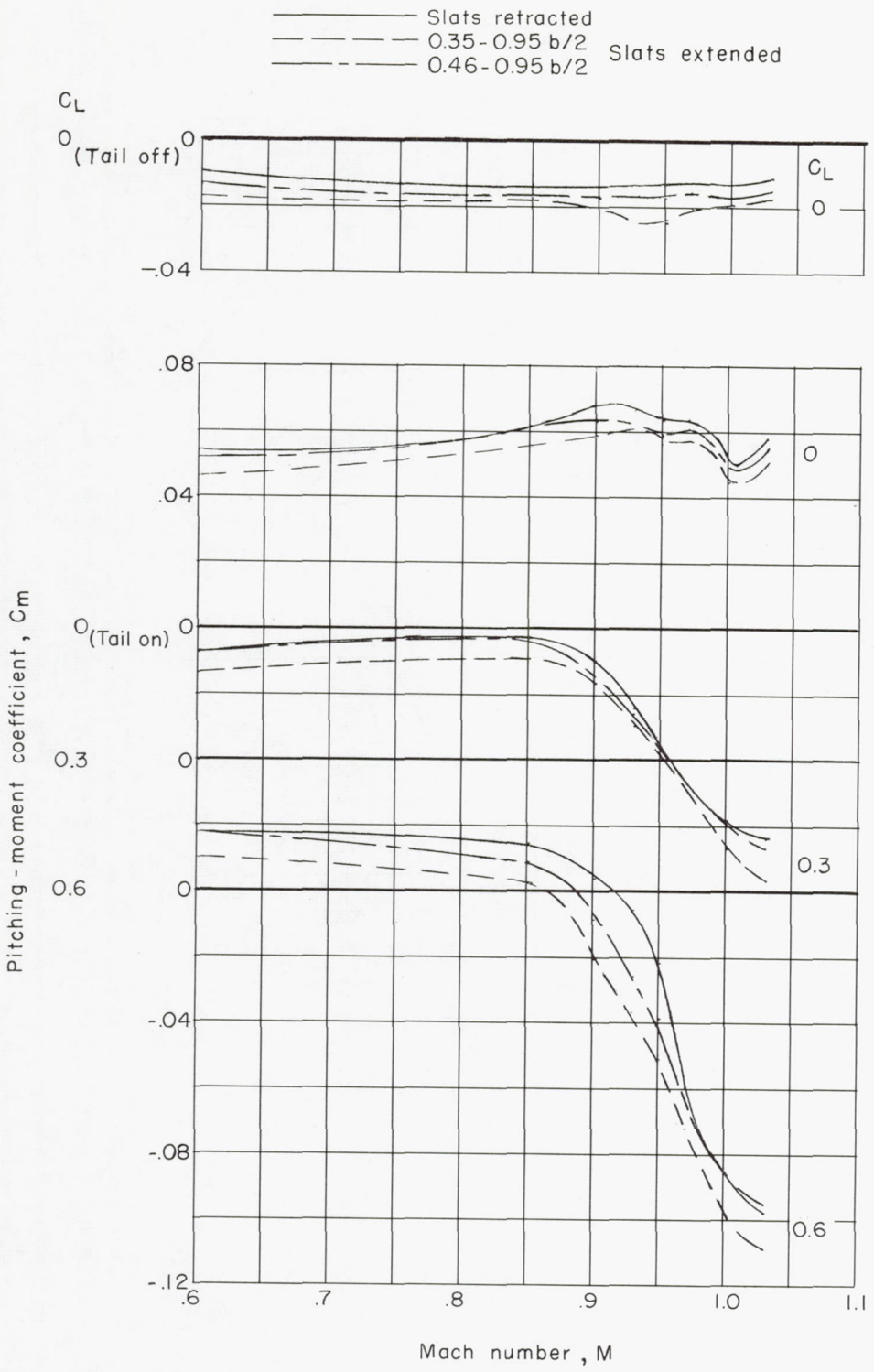

Figure 17.- Effect of Mach number on pitching-moment coefficient for complete model at several lift coefficients and for tail-off configurations at zero lift.

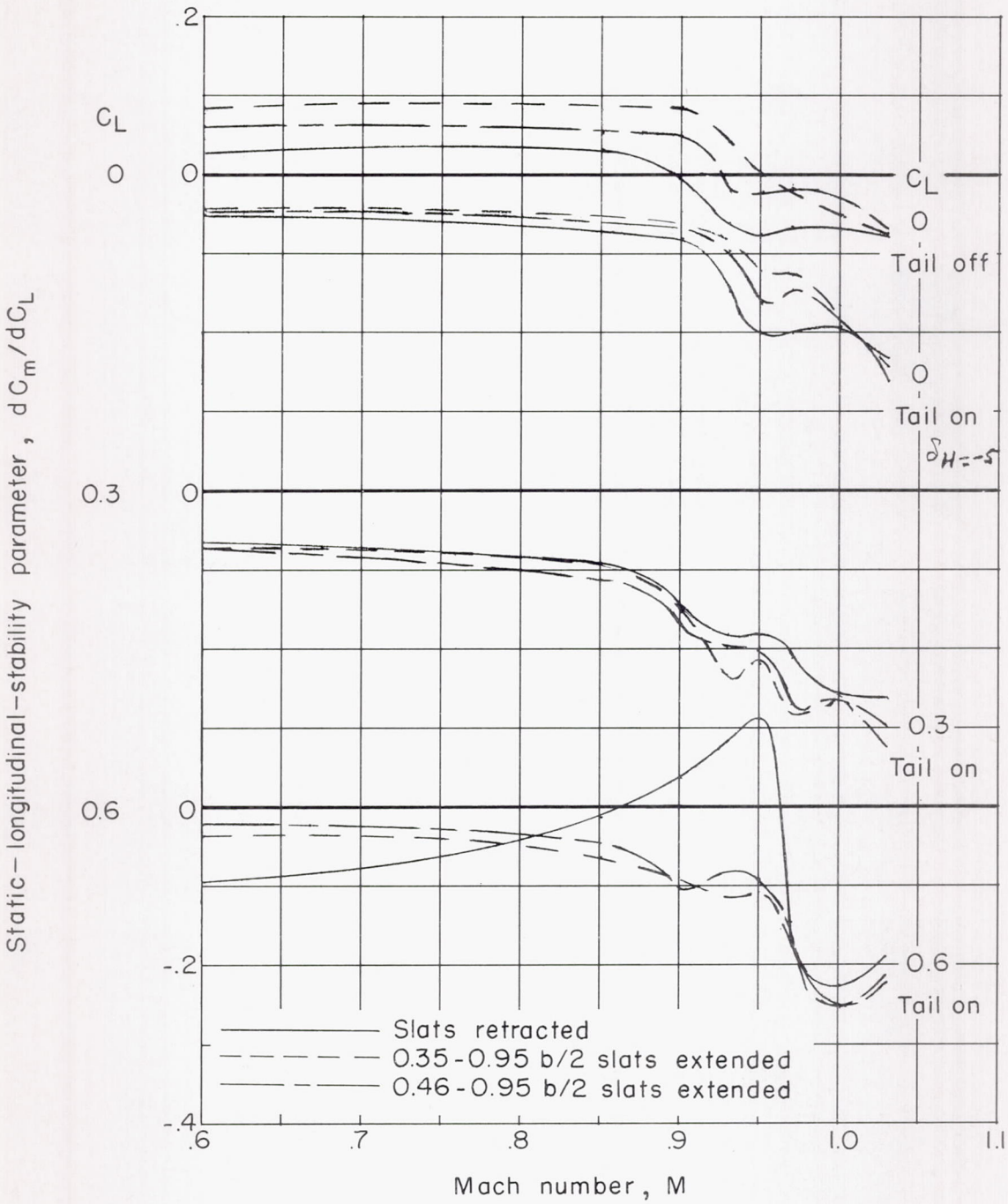

Figure 18.- Effect of Mach number on static-longitudinal-stability parameter for complete model at several lift coefficients and for tail-off configurations at zero lift.

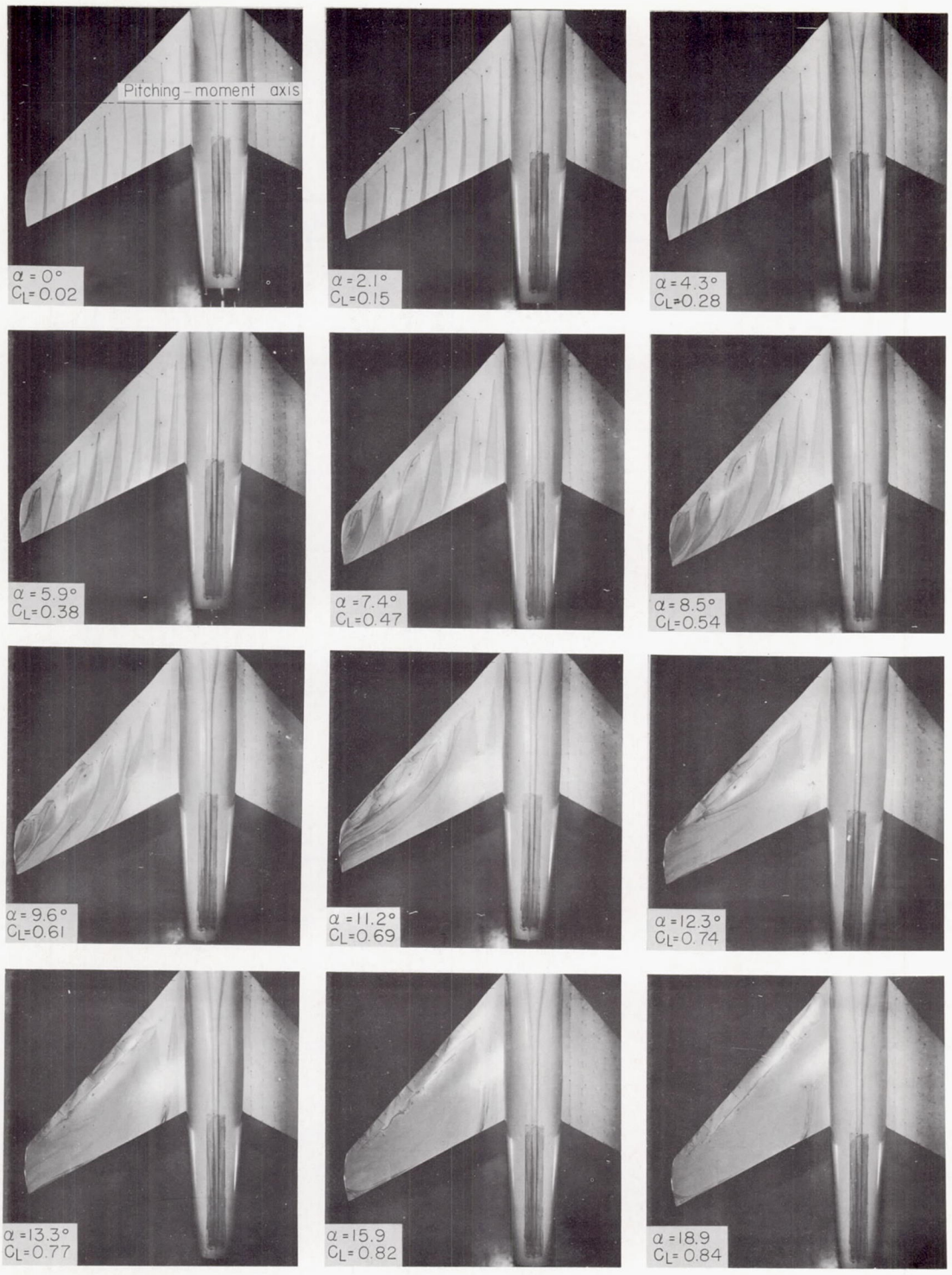

L-81238

(a) Slats retracted.

Figure 19.- Ink-flow photographs. Tail-off configuration. M = 0.60.

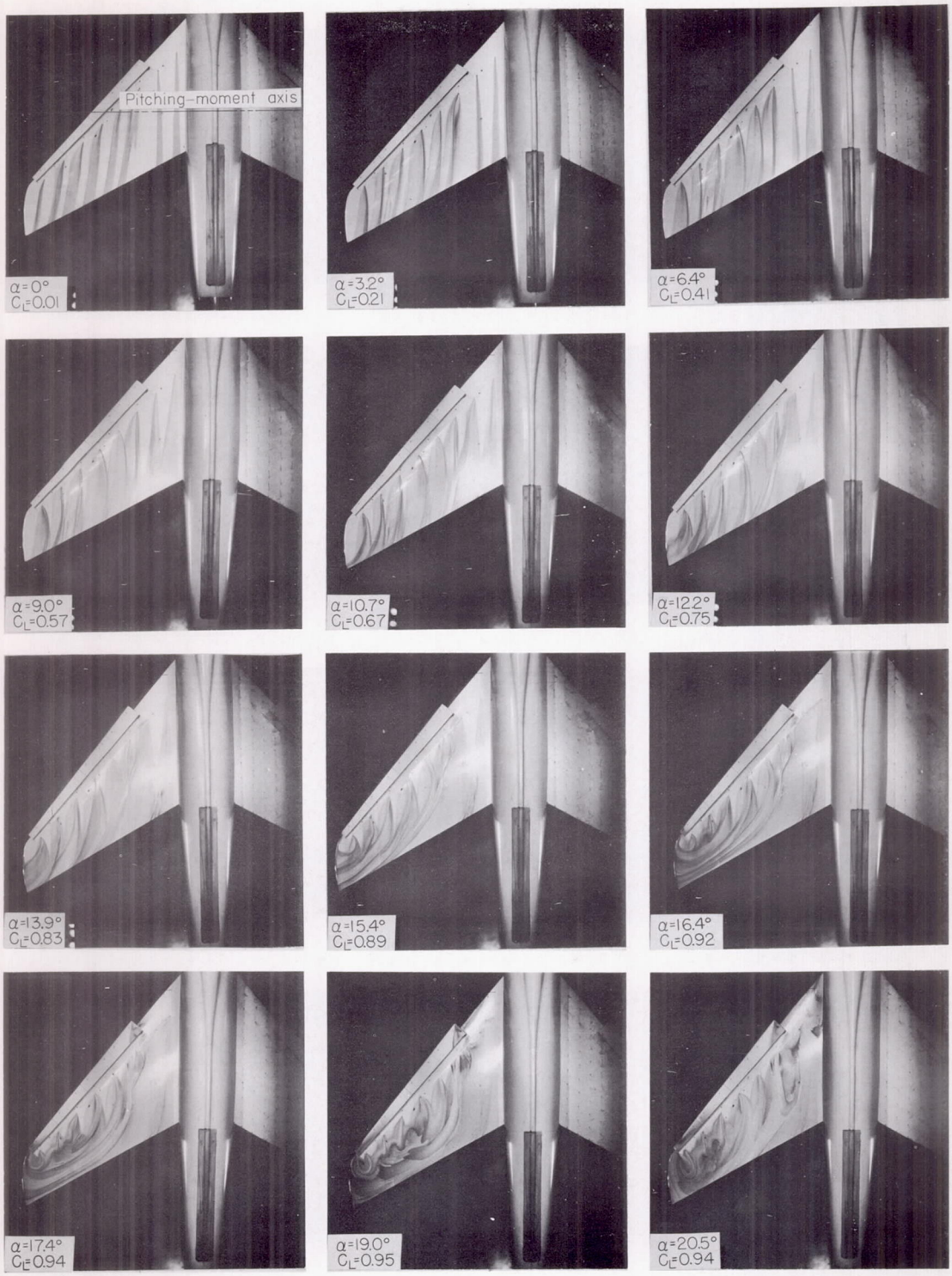

L-81239

(b) 0.35b/2 to 0.95b/2 slats extended.

Figure 19.- Concluded.

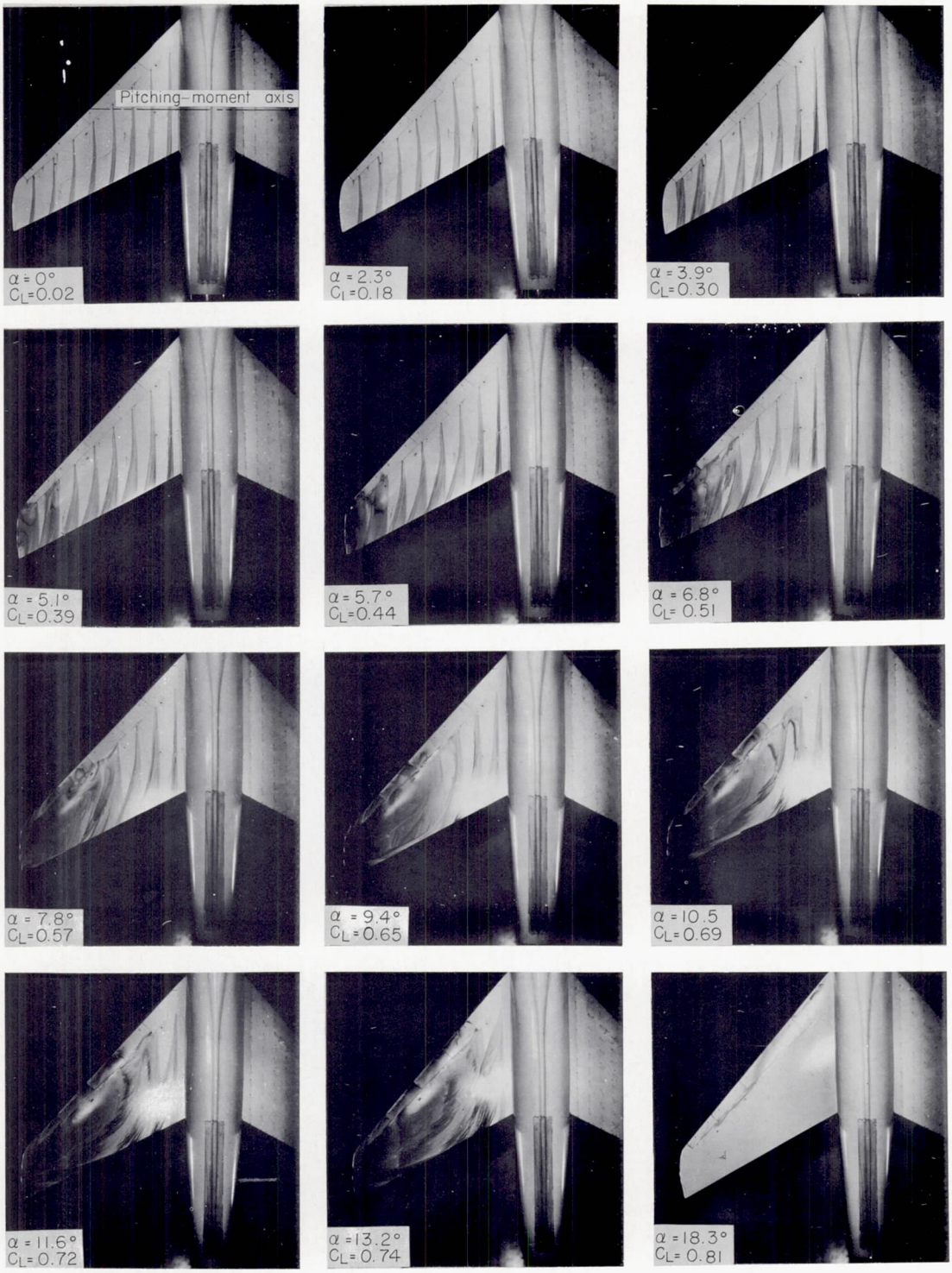

L-81240

(a) Slats retracted.

Figure 20.- Ink-flow photographs. Tail-off configuration. M = 0.85.

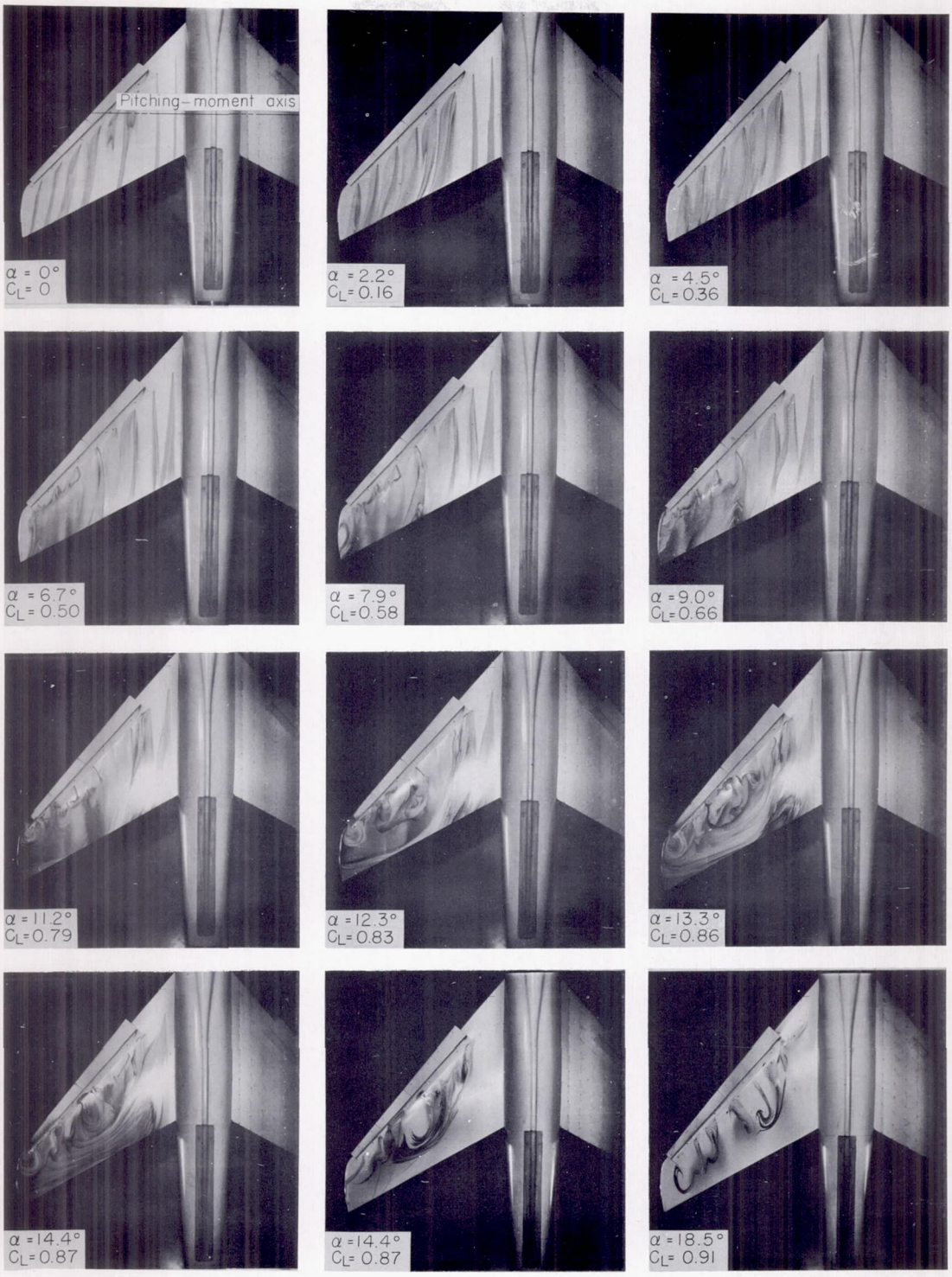

L-81241

(b) 0.35b/2 to 0.95b/2 slats extended.

Figure 20.- Concluded.

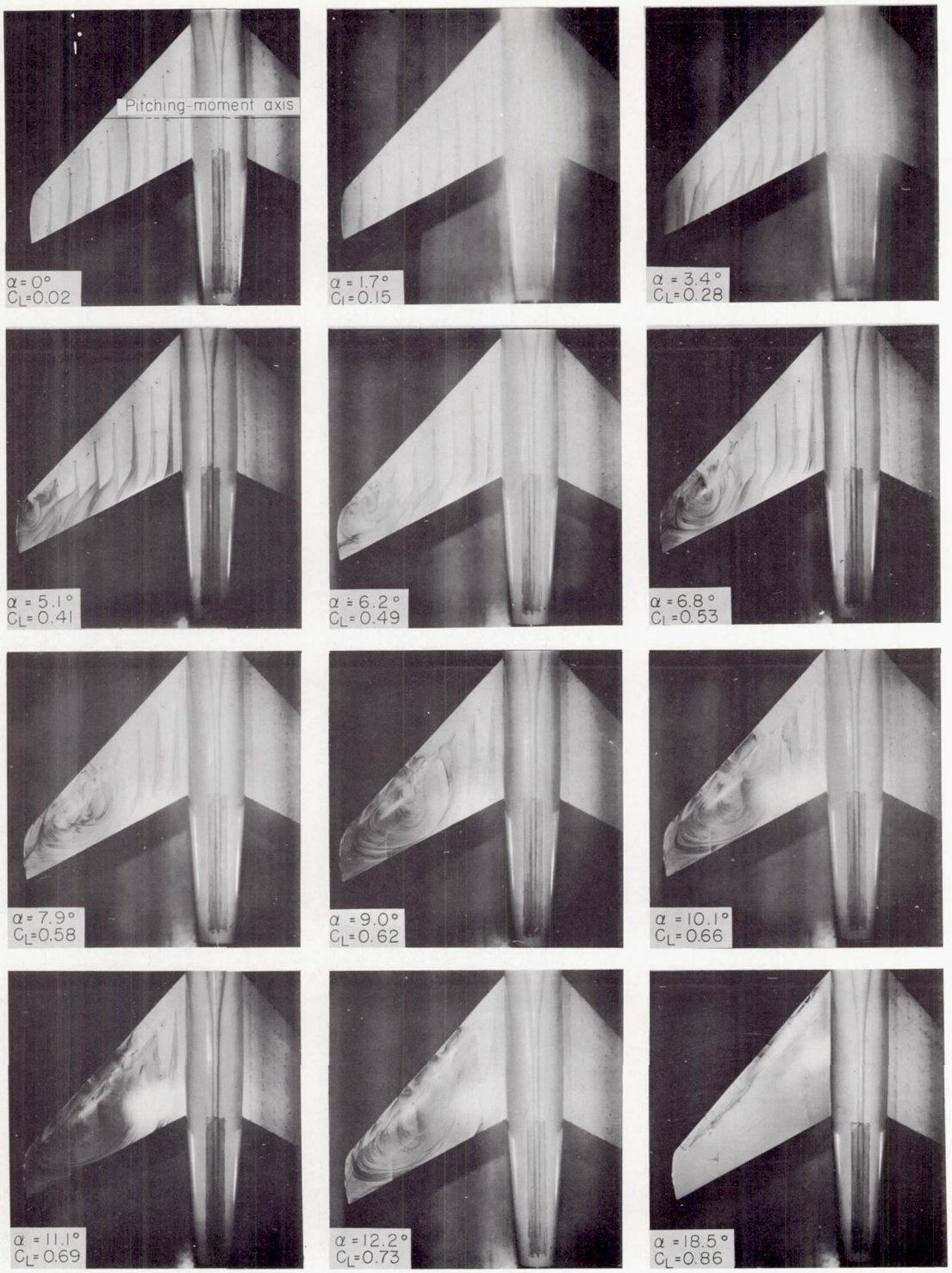

L-81242

(a) Slats retracted.

Figure 21.- Ink-flow photographs. Tail-off configuration. M = 0.90.

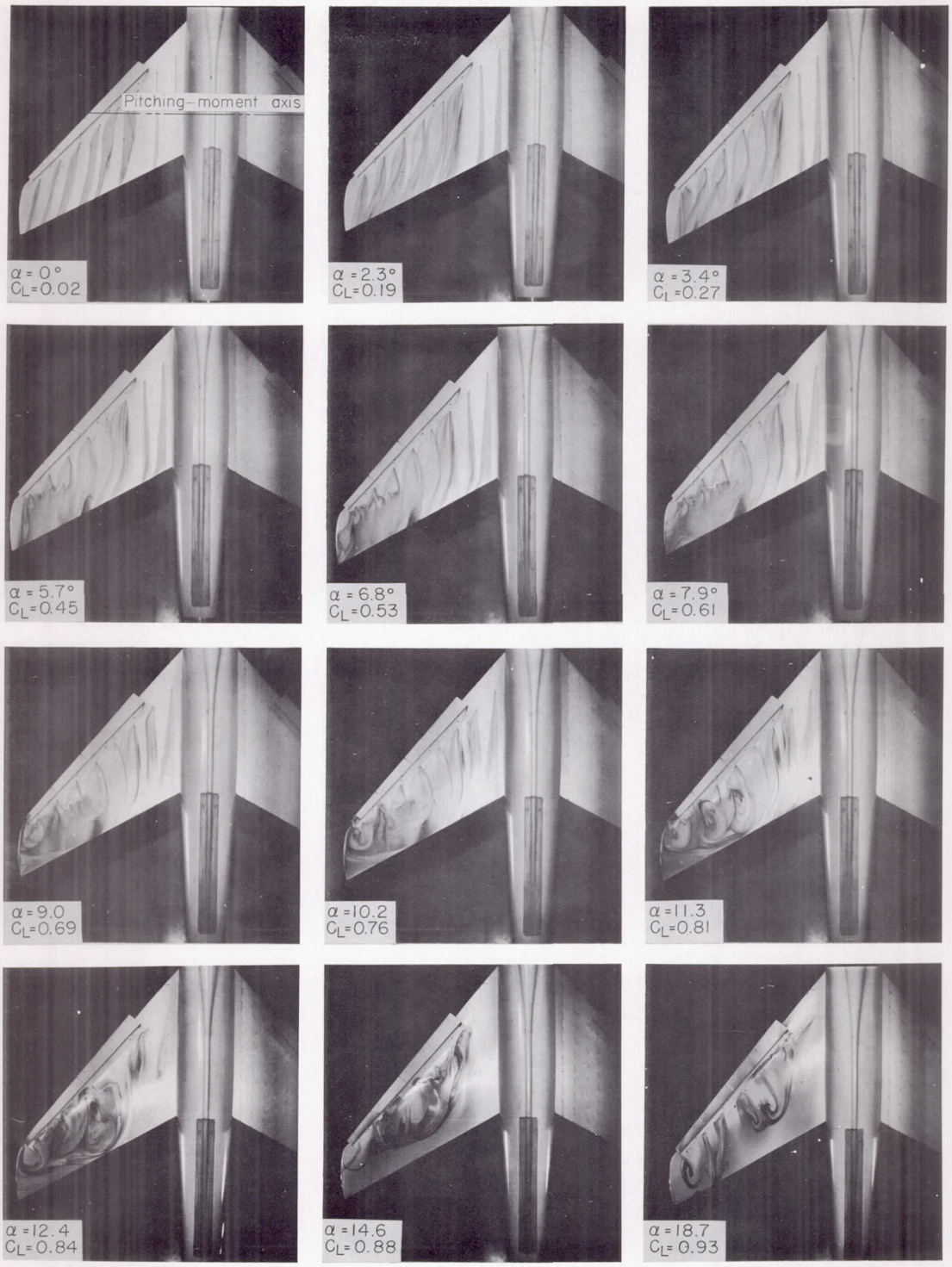

L-81243

(b) 0.35b/2 to 0.95b/2 slats extended.

Figure 21.- Concluded.

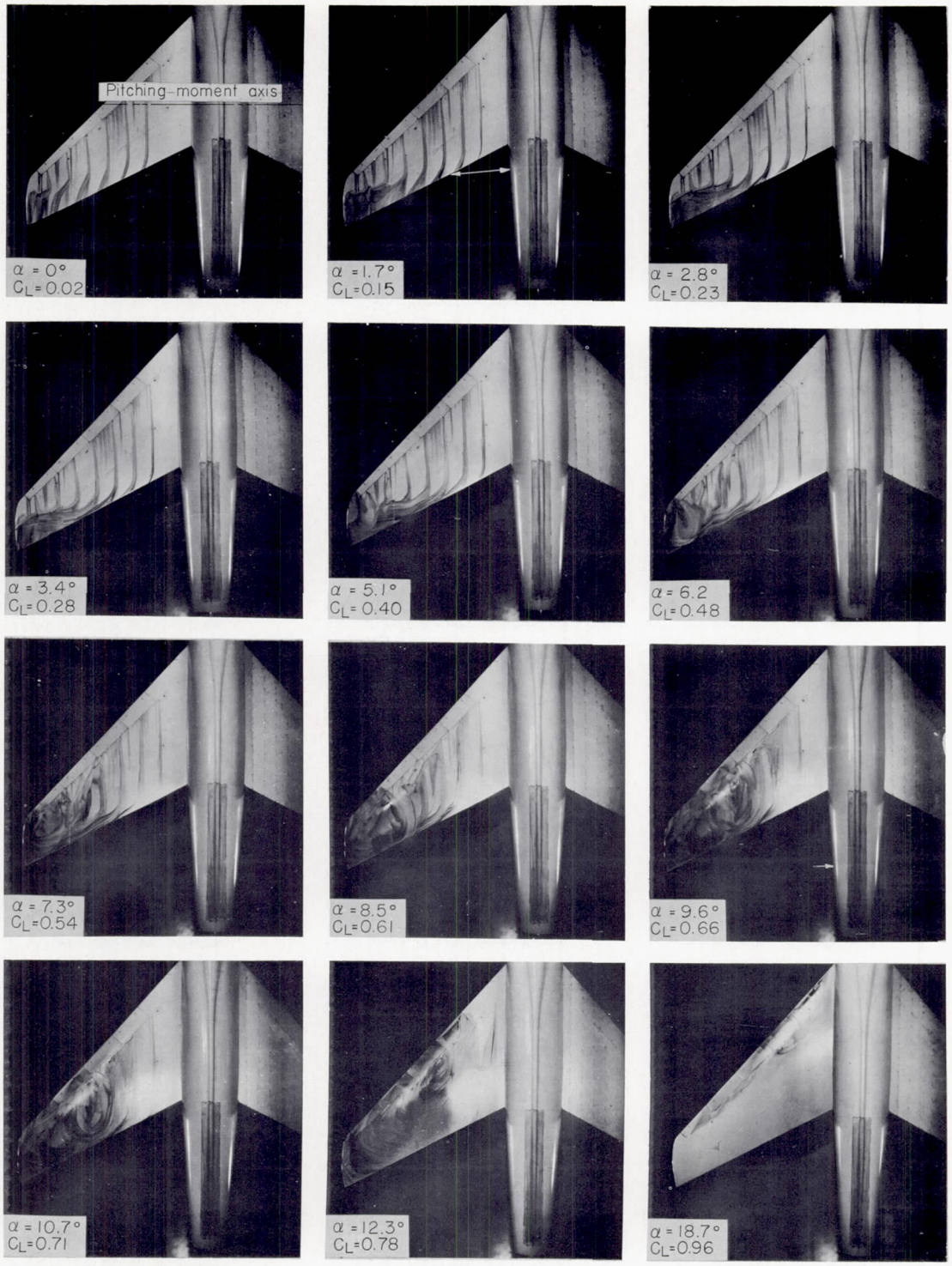

L-81244

(a) Slats retracted.

Figure 22.- Ink-flow photographs. Tail-off configuration. M = 0.95.

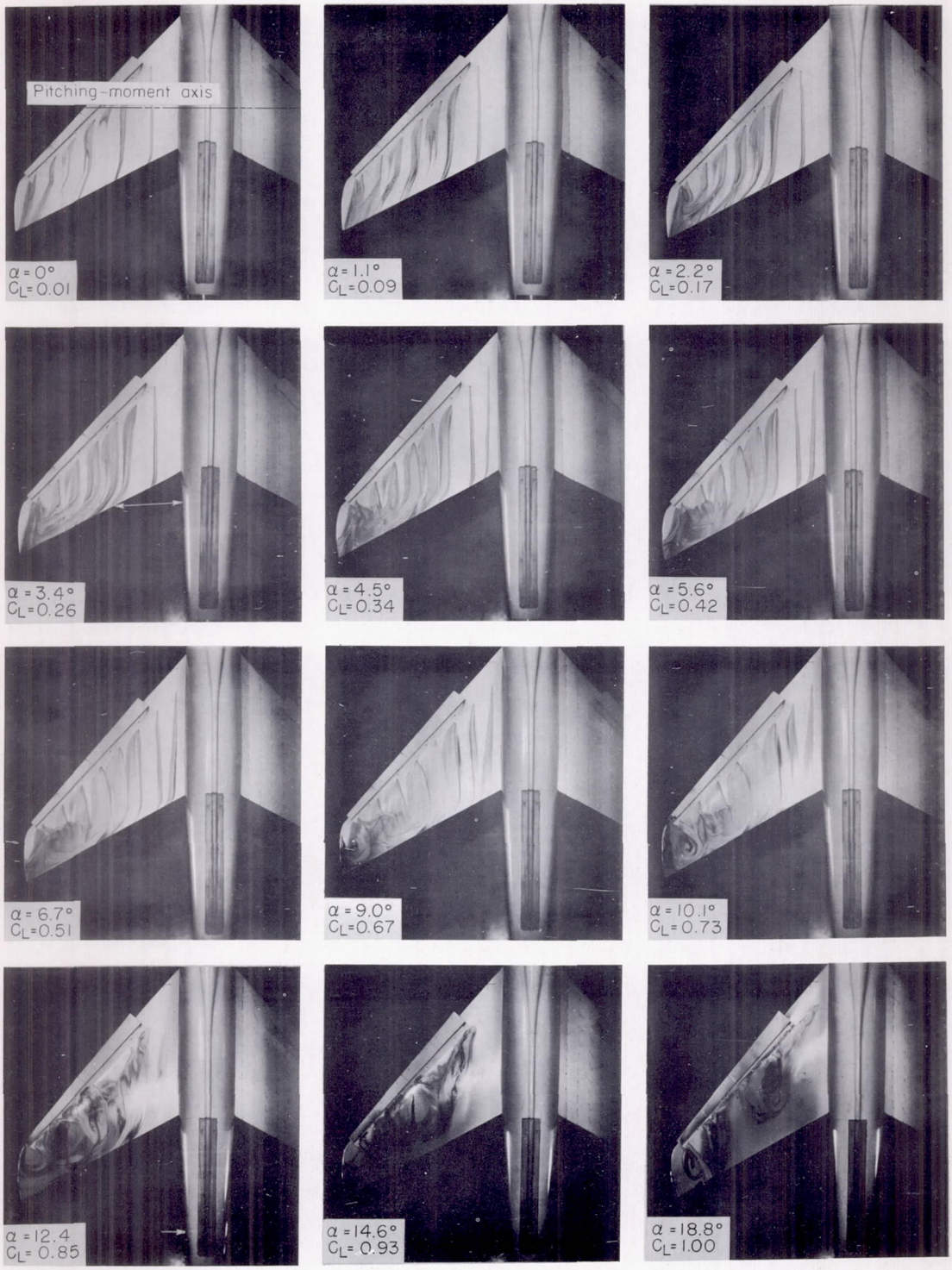

L-81245

(b) 0.35b/2 to 0.95b/2 slats extended.

Figure 22.- Concluded.

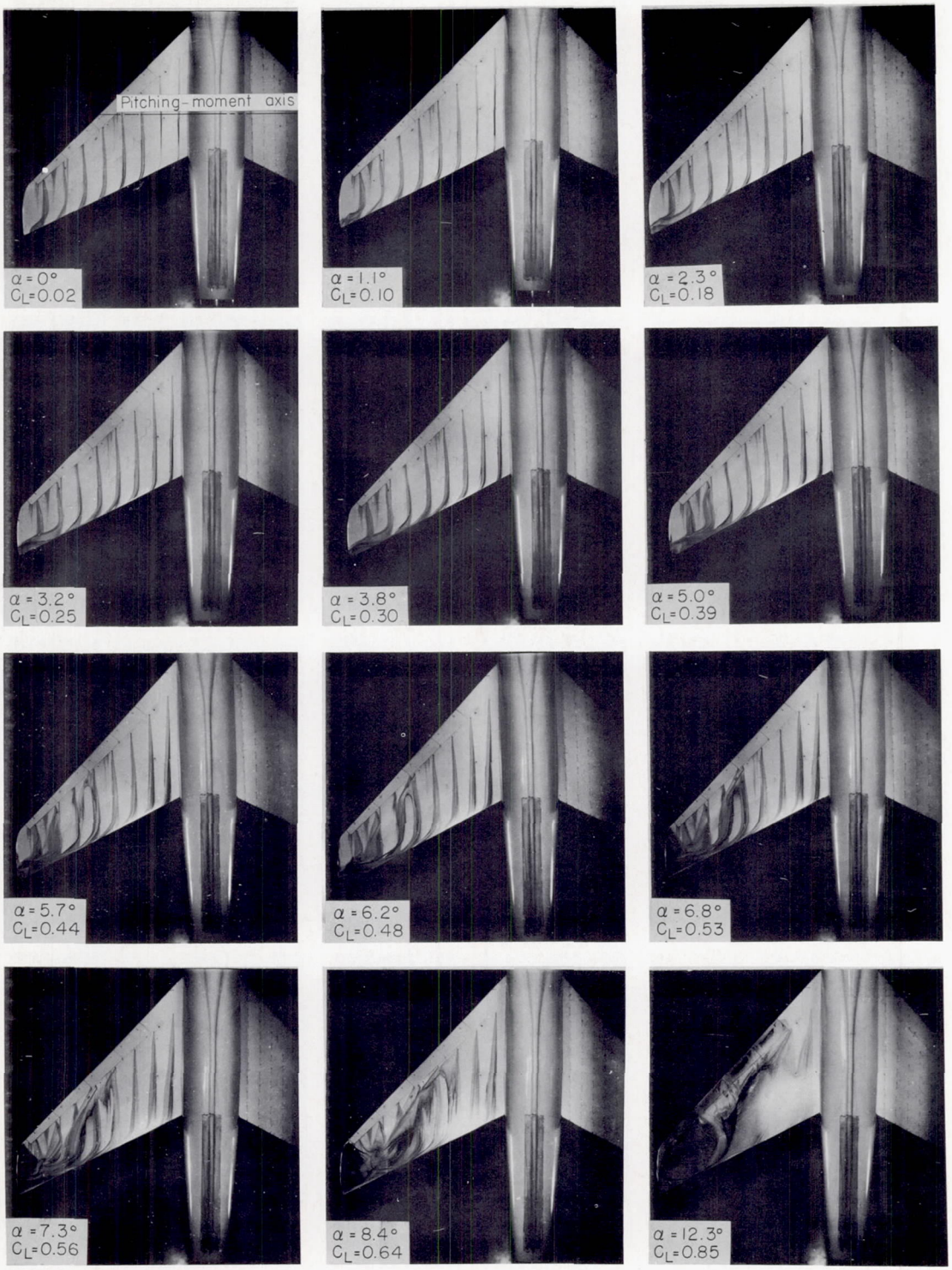

L-81246

(a) Slats retracted.

Figure 23.- Ink-flow photographs. Tail-off configuration. M = 1.00.

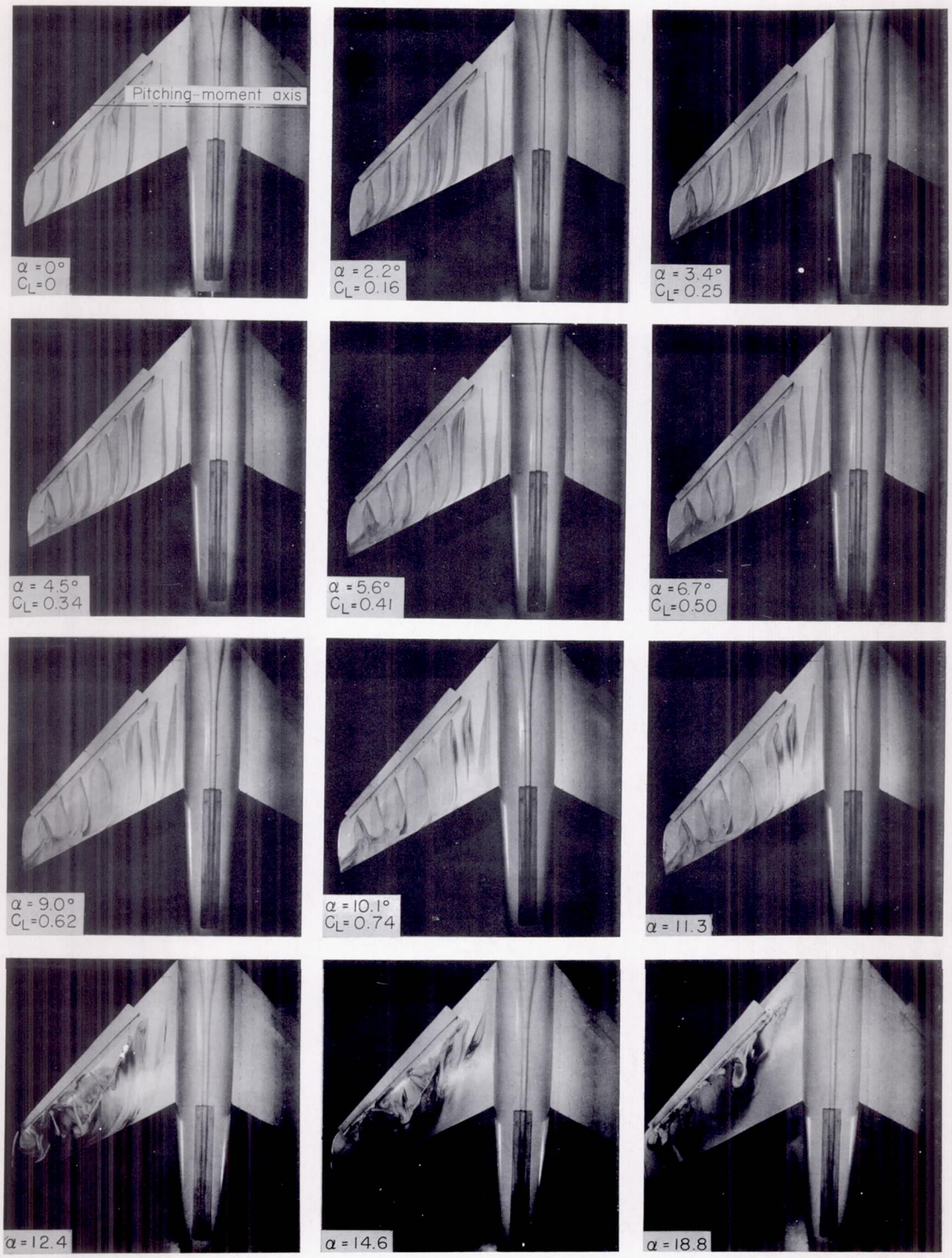

L-81247

(b) 0.35b/2 to 0.95b/2 slats extended.

Figure 23.- Concluded.

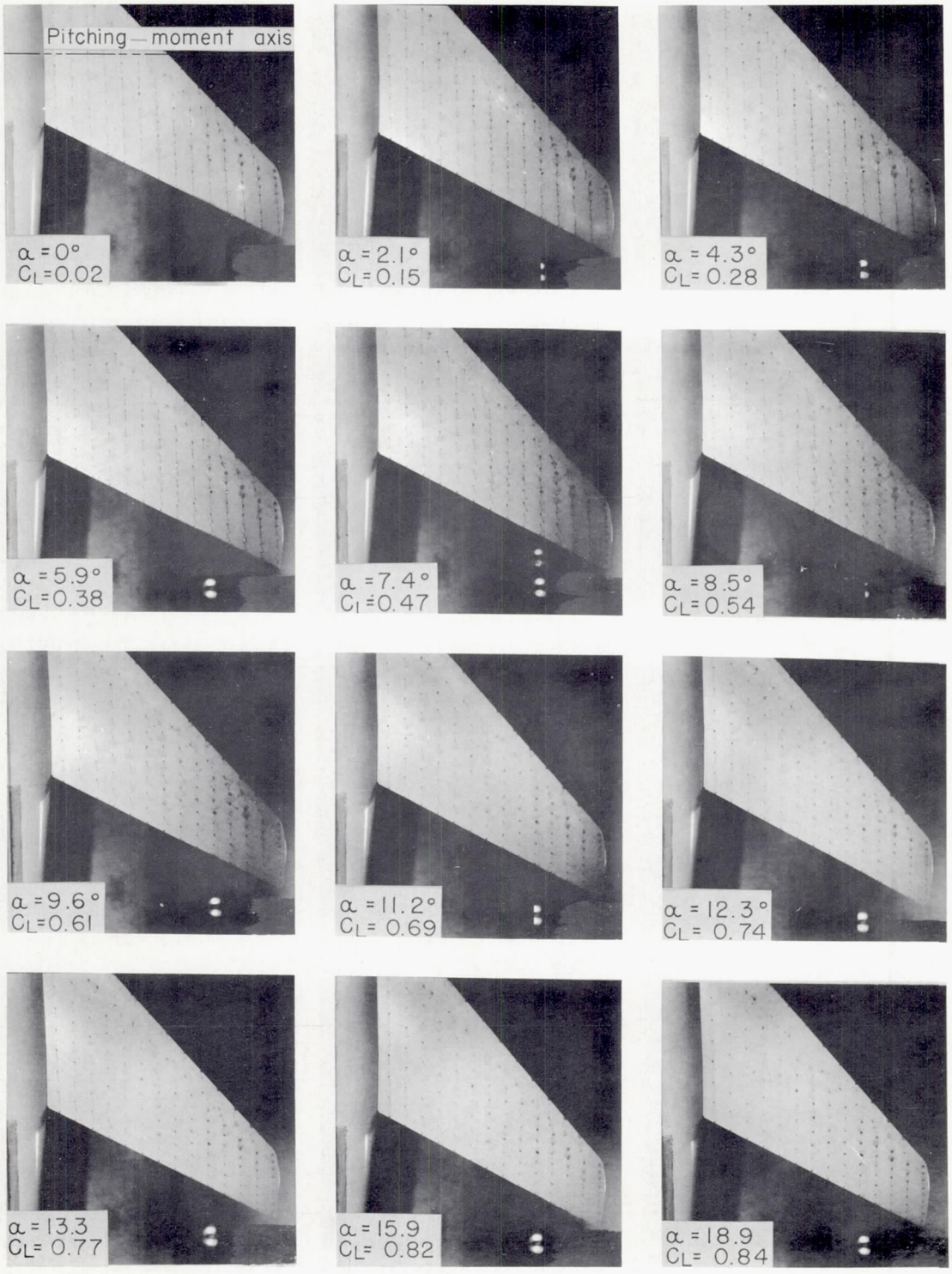

L-81248

(a) Slats retracted.

Figure 24.- Tuft photographs. Tail-off configuration. M = 0.60.

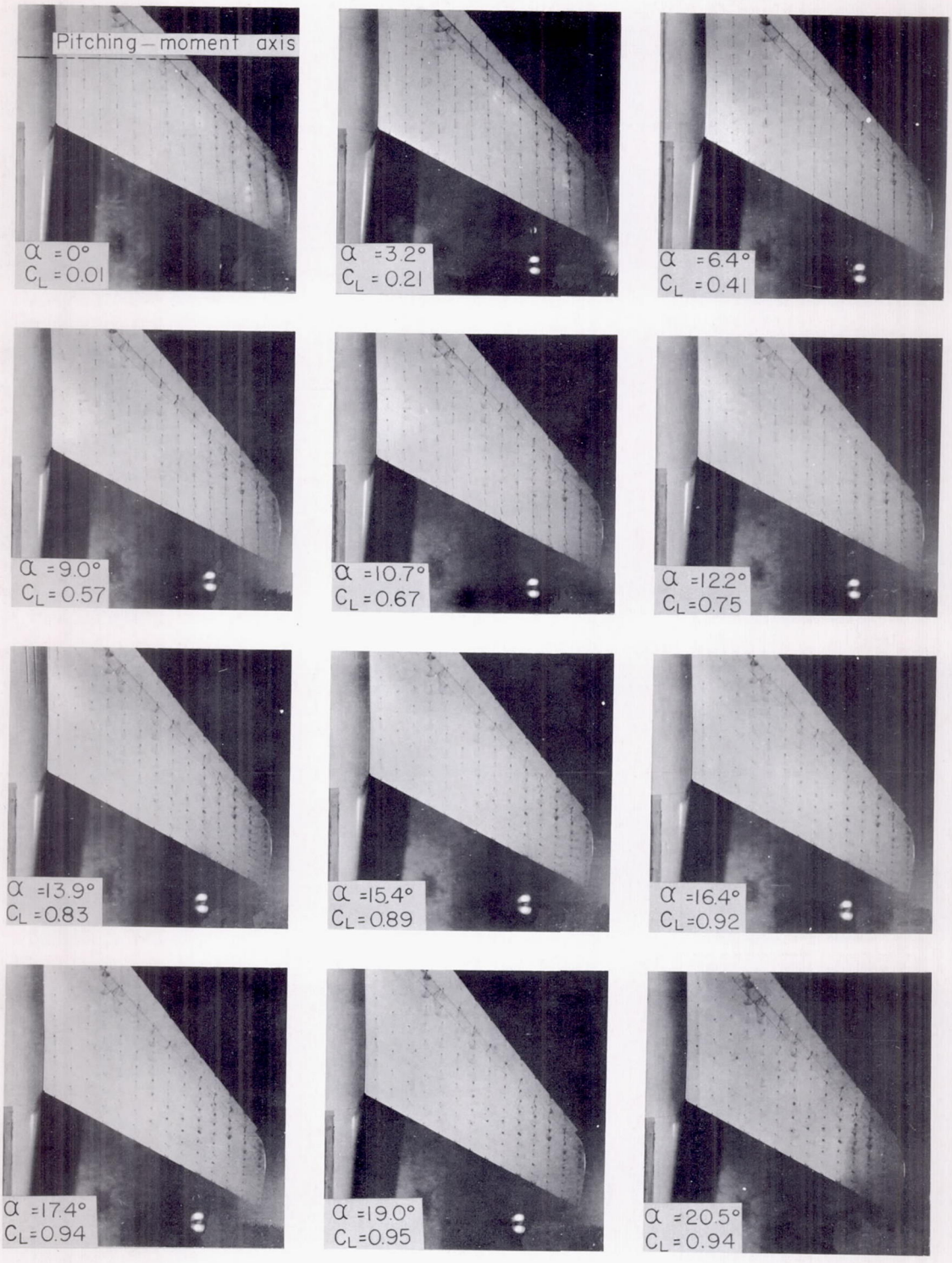

L-81249

(b) 0.35b/2 to 0.95b/2 slats extended.

Figure 24.- Concluded.

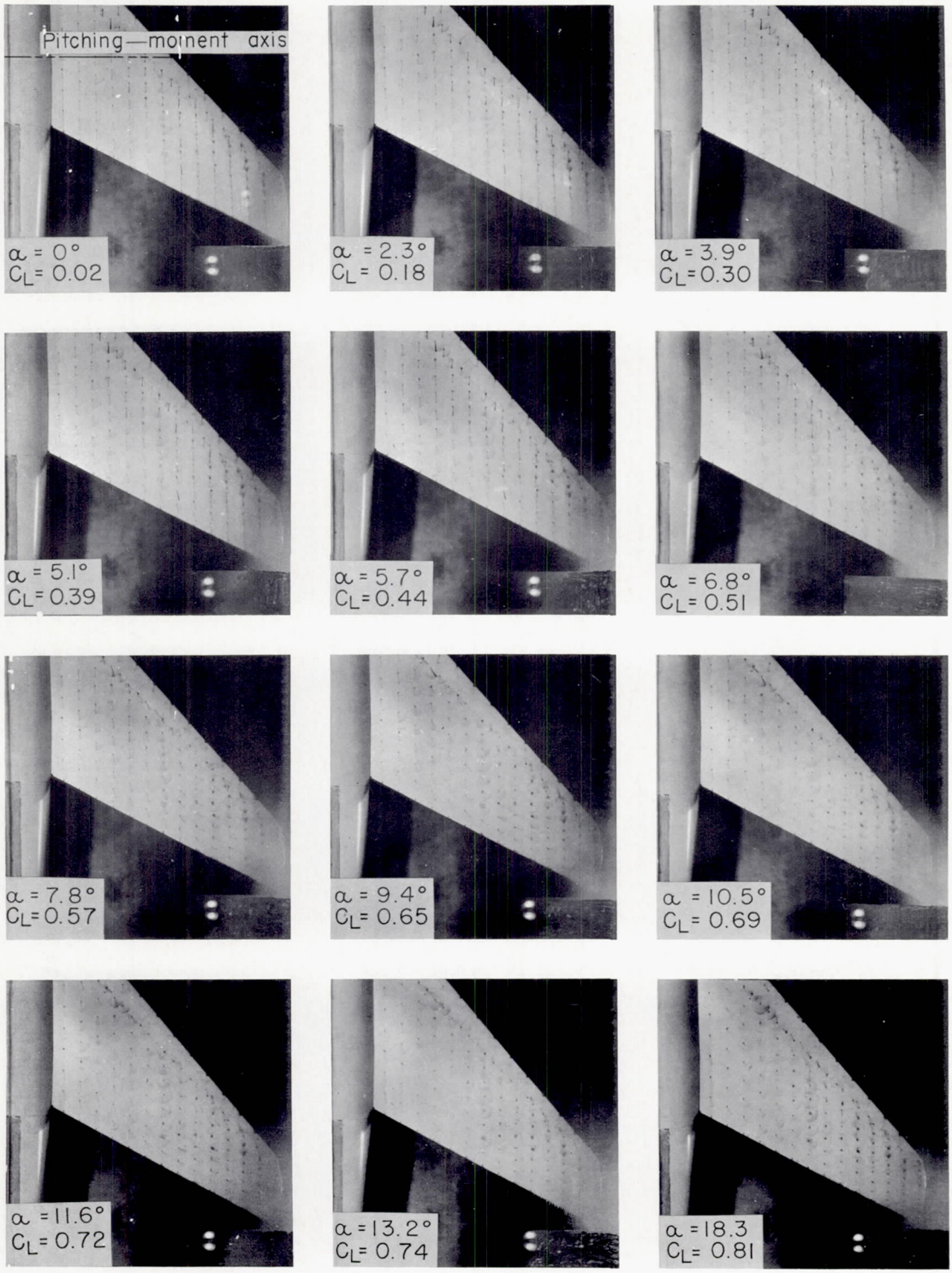

L-81250

(a) Slats retracted.

Figure 25.- Tuft photographs. Tail-off configuration. M = 0.85.

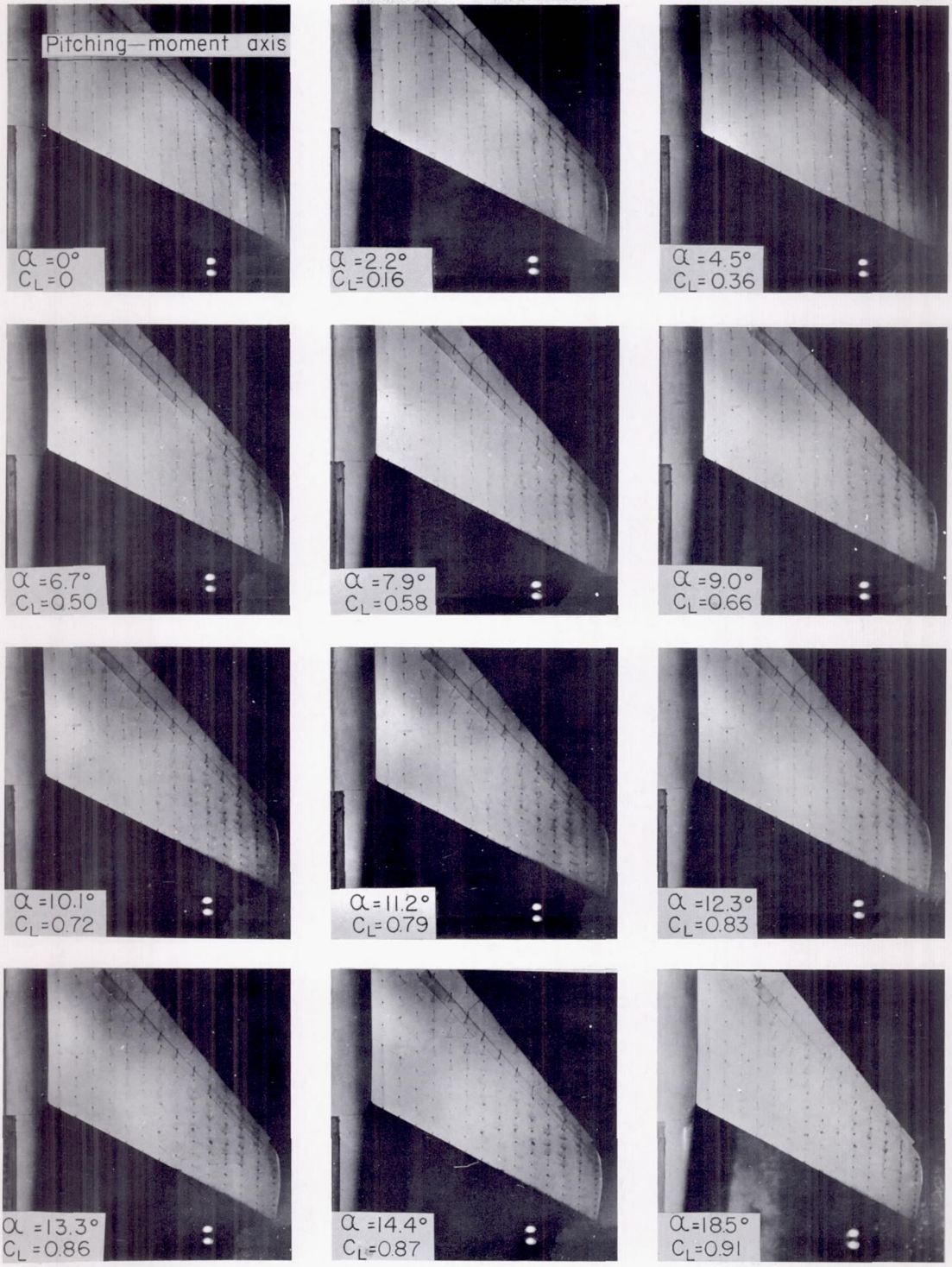

L-81251

(b) 0.35b/2 to 0.95b/2 slats extended.

Figure 25.- Concluded.

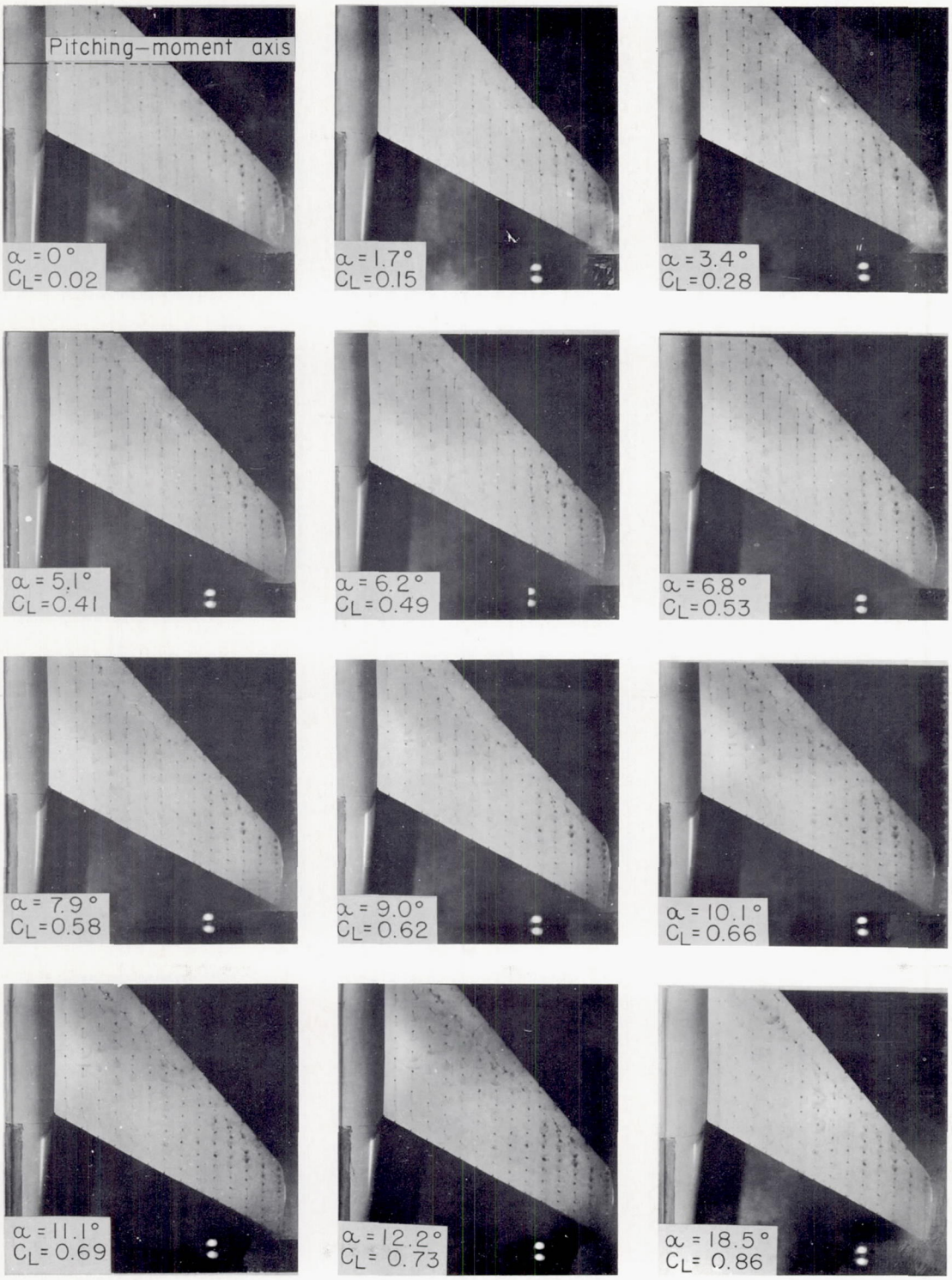

L-81252

(a) Slats retracted.

Figure 26.- Tuft photographs. Tail-off configurations. M = 0.90.

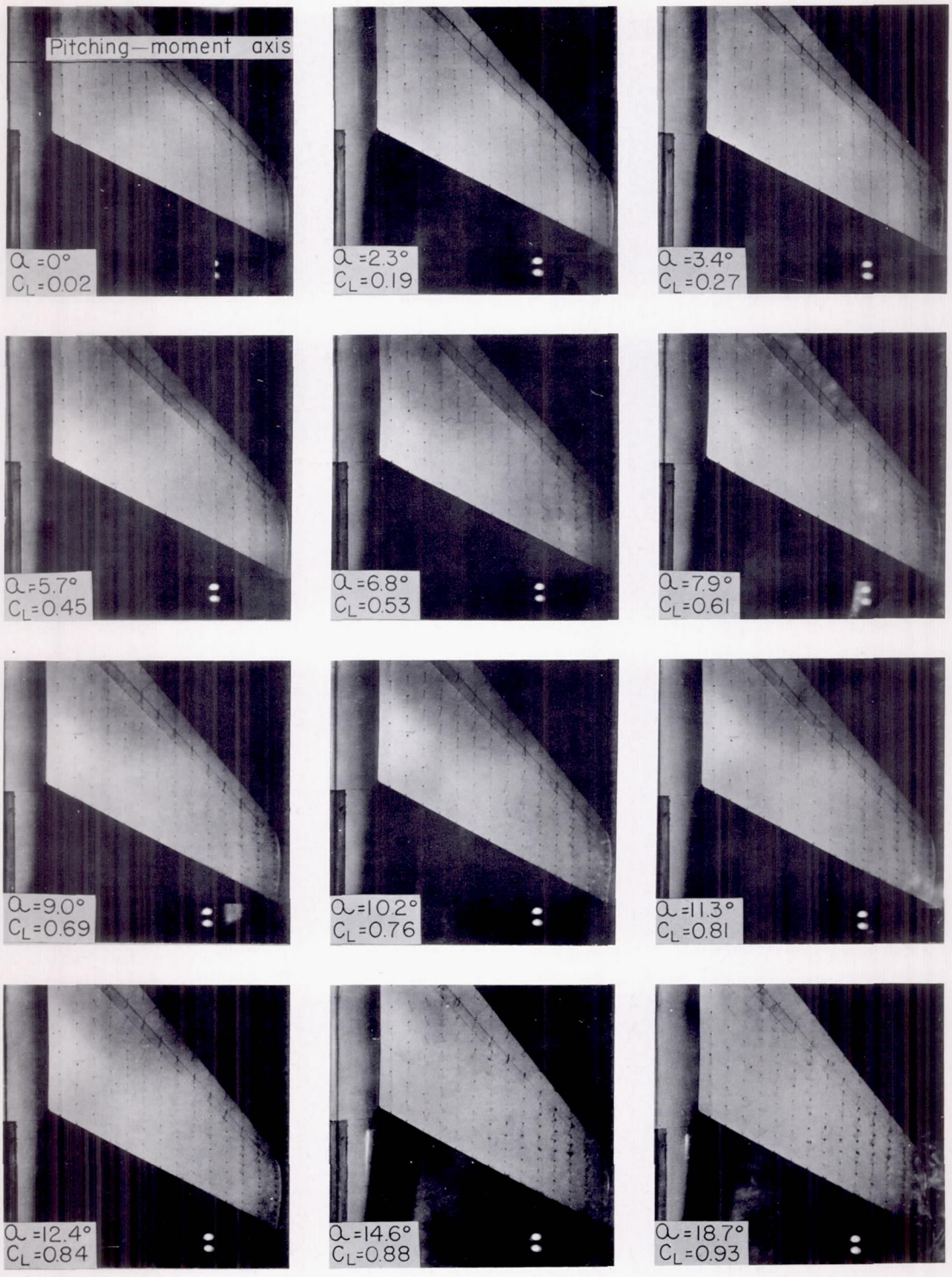

L-81253

(b) 0.35b/2 to 0.95b/2 slats extended.

Figure 26.- Concluded.

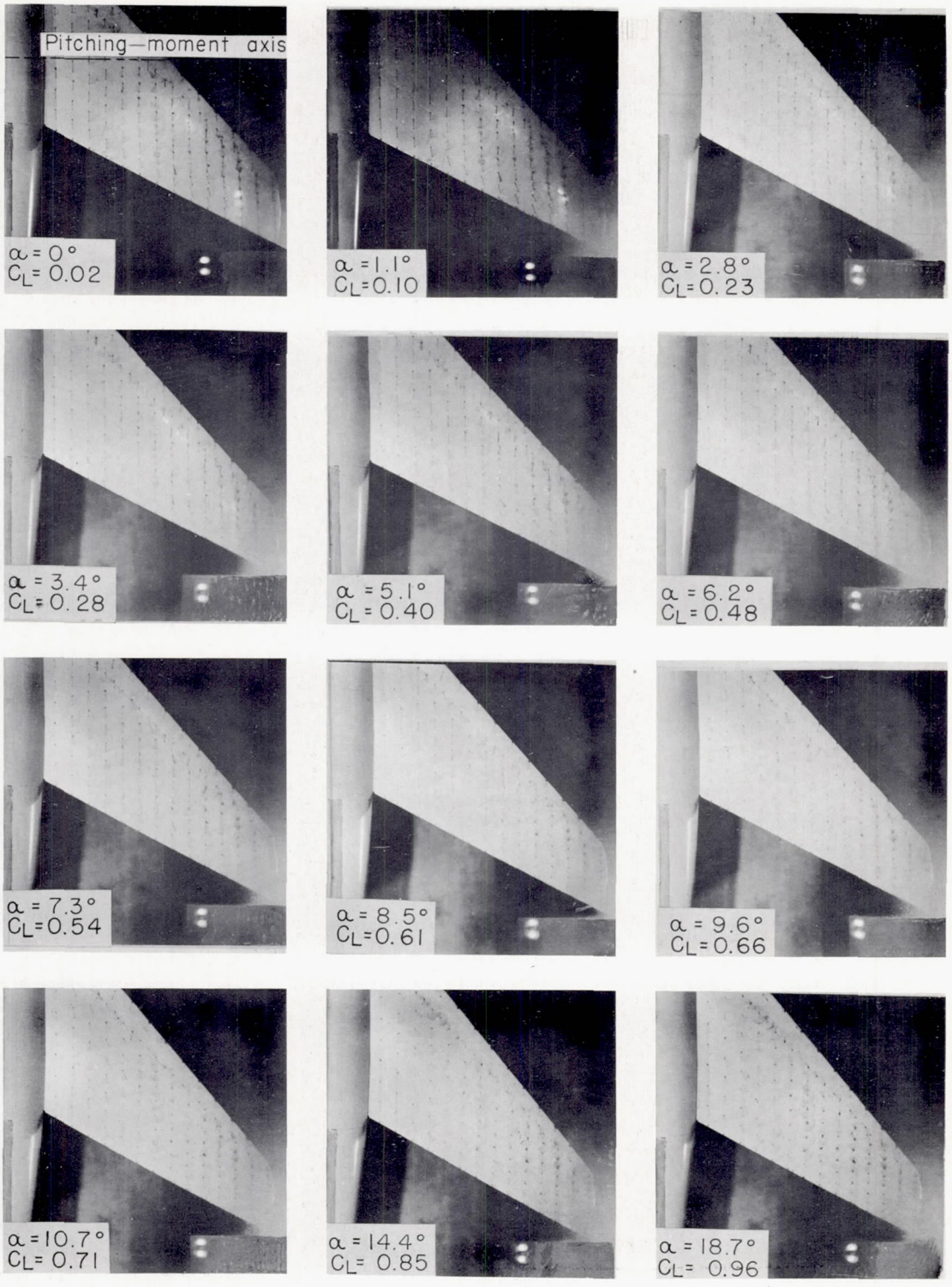

L-81254

(a) Slats retracted.

Figure 27.- Tuft photographs. Tail-off configuration. M = 0.95.

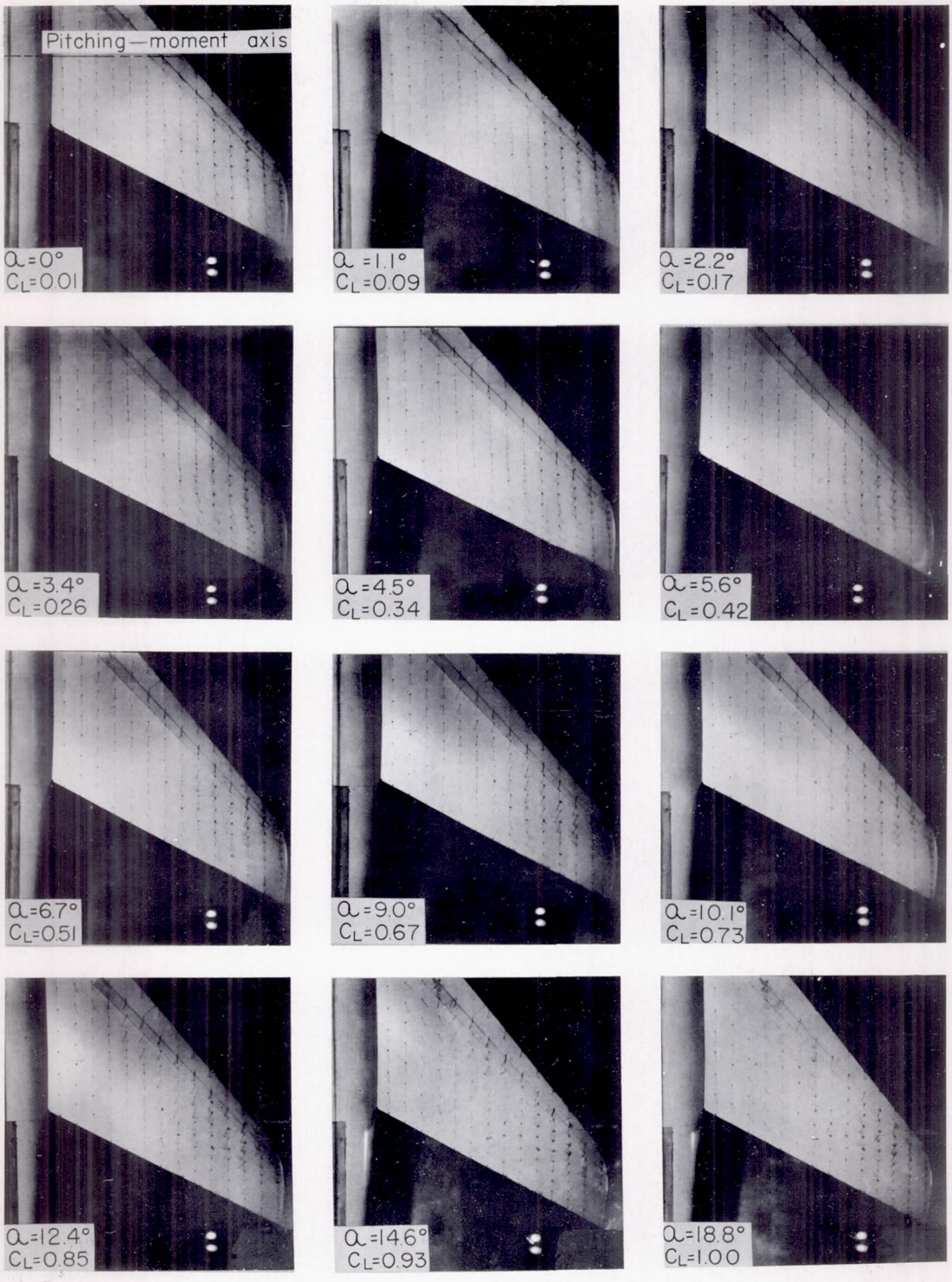

L-81255

(b) 0.35b/2 to 0.95b/2 slats extended.

Figure 27.- Concluded.

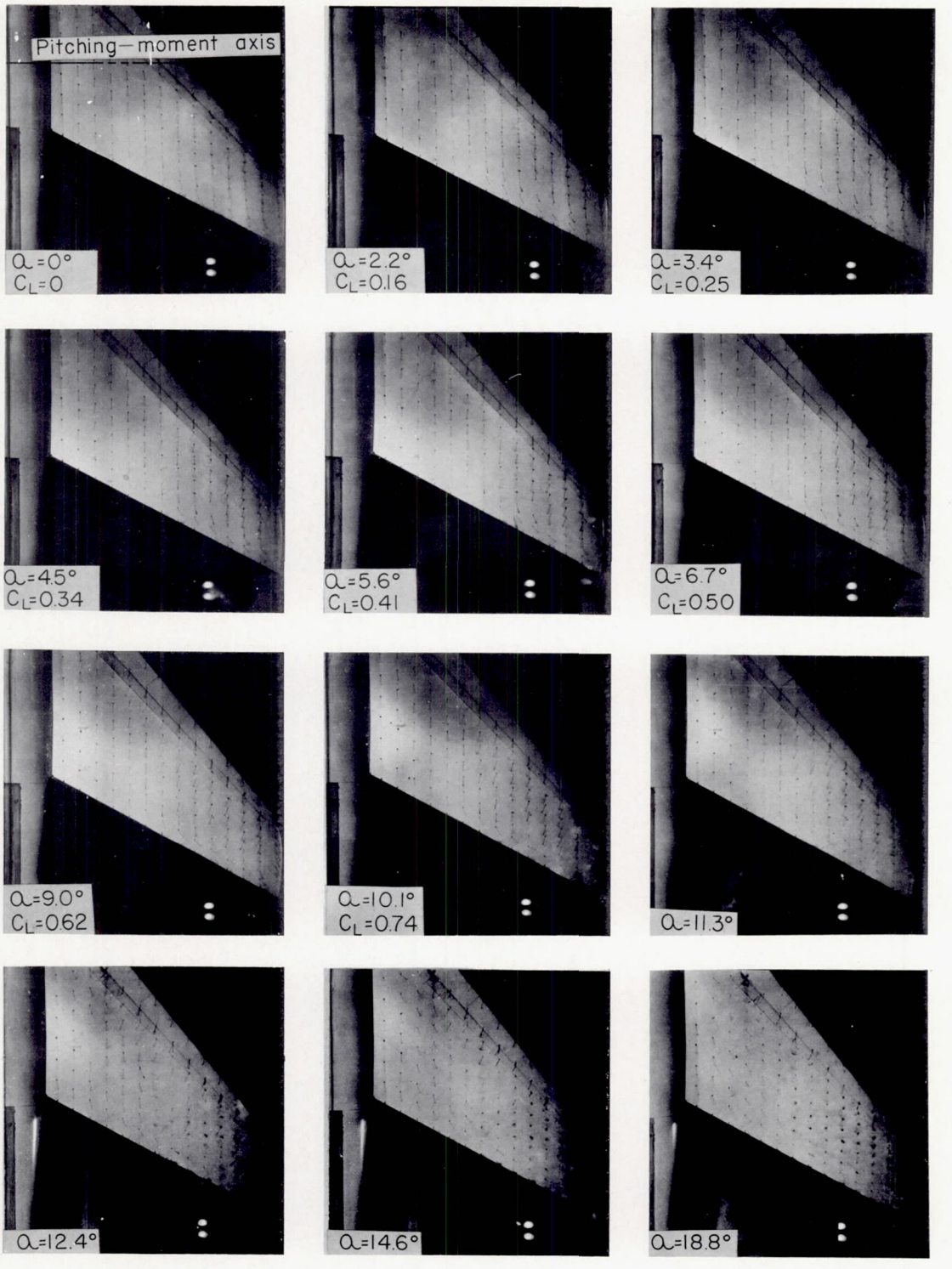

L-81256

Figure 28.- Tuft photographs. Tail-off configuration. M = 1.00. 0.35b/2 to 0.95b/2 slats extended.

NACA-Langley - 4-5-54 - 325